rijksuniversiteit groningen

Review Paper •WMNS011-06•
Faculty of Science and Engineer
Zernike Institute for Advance Materials
University of Groningen

Spin Hall magnetoresistence for electronic determination of magnetic ordering

Gustavo Chávez Ponce de León (S4614771) & H.A.M.S. ter Tisha
Email: g.chavez.ponce.de.leon@student.rug.nl
April 2022

Abstract

When a non-magnetic conductor is in contact with a magnetic insulator, the resistance of the conductor is modulated by the magnetization direction in the insulator. This effect is known as the Spin Hall Magnetoresistence. The current theory of the Spin Hall Magnetoresistence relates this phenomenon to a non-equilibrium spin accumulation at the interface accompanied by the simultaneous action of the Spin Hall and Inverse Spin Hall Effects. In this work, we review this theory emphasizing later modifications introduced to explain a significant disagreement between theory and experiments on non-collinear magnets. In addition, we explore the possibility of employing this magnetoresistence for applications in next-generation spintronics, such as the purely electrical detection of complex magnetic textures.

Contents

1 Introduction

In his 1959 seminal talk *"There's Plenty of Room at the Bottom"*, Richard P. Feynman presented to the American Physical Society the following idea: if one were to store information using a binary system in which each bit consist of a 5x5x5-atoms cube of either silver or gold, all of the information from all of the books in the world could be written in a cube of material no bigger than the smallest spec of dust the human eye can see [1].

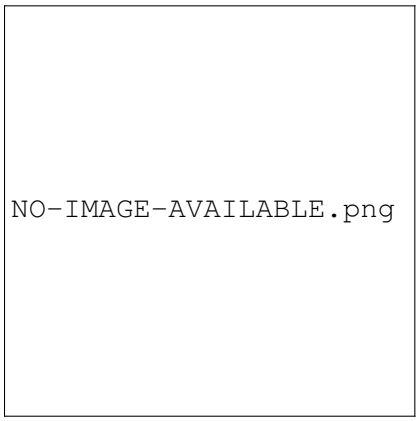

Figure 1: *Exponential growth of areal density storage (update 2022). Note that 1000GiB = 125GB. Image taken from [2].*

Although we are still far from the length scales Feynman envisioned, there is no doubt that the density at which information can be stored has experienced a tremendous and consistent exponential growth during the last few decades (see Fig. 1) [2, 3]. In 1959 —the year of Feynman's speech— the state-of-the-art computers could store merely 132 bytes per in^2 [4–6]. In contrast, current hard disk drives [HDD] can easily store more than 120GB per in^2 [3, 7]. A 10^9-fold increment in areal density!

This massive increase in storage density has created industrial sectors worth billion with growing markets [8]. Undoubtedly, a key factor in this success story has been the pursue of miniaturization in electronics components [3, 9, 10]. However, miniaturization brings new scientific and technological challenges as it approaches nanometer scales. At those scales heat dissipation becomes crucial: it negatively impacts device lifetime and reliability [10, 11]. Furthermore, thermal fluctuations impose fundamental physical limits[1], which restricts the scales and efficiencies achievable with conventional design strategies [12–14]. Aiming to sustain the present growth in information density, researchers have spent the last few decades exploring novel and unconventional properties of matter for its use in memory devices [9]. In that regard, the field of spintronics stands out as a promising candidate for 21^{st}-century electronics [15, 16].

Unlike conventional electronics, which solely employs the electron charge, **spintronics** simultaneously employs both the electron spin and charge[2] [17]. Spintronics has evolved considerably since its origins in the late 80s [15], and today this field is developing into several roads to tackle the limitation of modern designs [17, 18]. One of such directions proposes the use of spin arrangements —called **skyrmions**— as information carriers [see Fig. 2] [19, 20]. This arrangements cannot be continuously deformed into a uniform magnetic state, and thus exhibit a property called **topological protection** [21, 22]. Therefore, skyrmions appear to be suitable candidates for ultra-dense memory and logic devices that could overcome current limits [22].

Nevertheless, several design challenges must be surmounted for a successful incorporation of these quasi-particles as information carriers. Primarily, techniques to easily create, transport, annihilate, and detect skyrmions are indispensable [23]. For instance, standard procedures to detect the presence of a magnetic order usually involve sophisticated techniques with enormous experimental set-ups such as neutron diffraction [24] or Lorentz transmission electron microscopy [LTEM] [25]. Not surprisingly, a considerable amount of research has been focused on developing simple and reliable detection methods. In particular, electrical detection is highly pursued since it could easily be incorporated with current electronics technology [26, 27]. In recent years, a new technique for an all-electrical detection of spin arrangements based on the **Spin Hall Magnetoresistence** [SMR] was put forward [28].

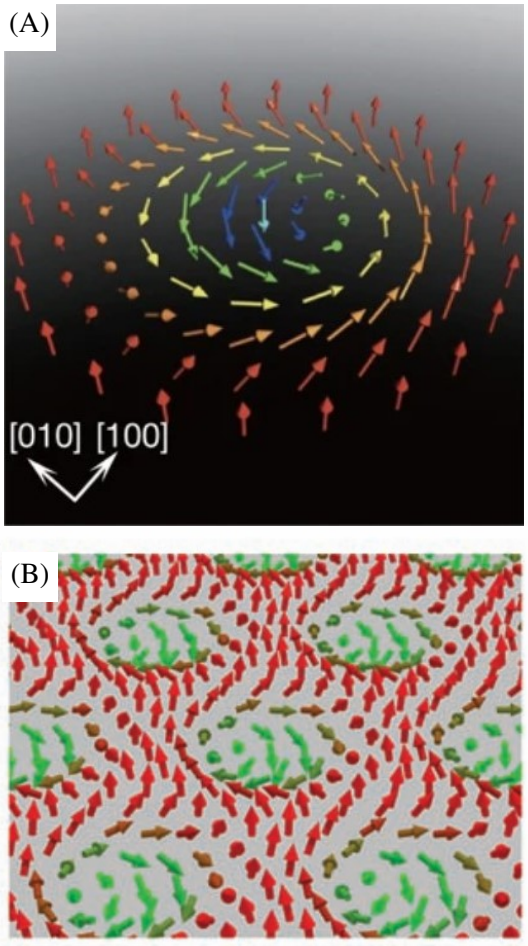

Figure 2: *(A) Schematic representation of the a single skyrmion. Image taken from [25]. (B) In the skyrmionic phase, the quasi-particles arrange in a honeycomb structure. Image taken from Ref. [24].*

SMR is a new type of magnetoresistence which was inadvertently detected for the first time by Weiler *et al.* [29, 30] in 2012. They noticed that the resistance of a platinum [Pt] layer deposited on top of the ferrimagnetic insulator made of yittrium iron garnets $Ye_3Fe_5O_{12}$ [YIG] was affected by the

[1] For magnetic storage, this limit is known as the superparamagnetic limit.
[2] Spin + Electronics = Spintronics

direction of insulator's magnetization. Subsequent experiments carried out by Huang *et al.* [31] corroborated these findings. Originally, both groups [29, 31] attributed this effect to an induced magnetization created by the insulator in the Pt layer. The magnetized platinum layer would exhibit the standard Anisotropic Magnetoresistence [AMR][3]. Their findings are schematically illustrated in Fig. 3.

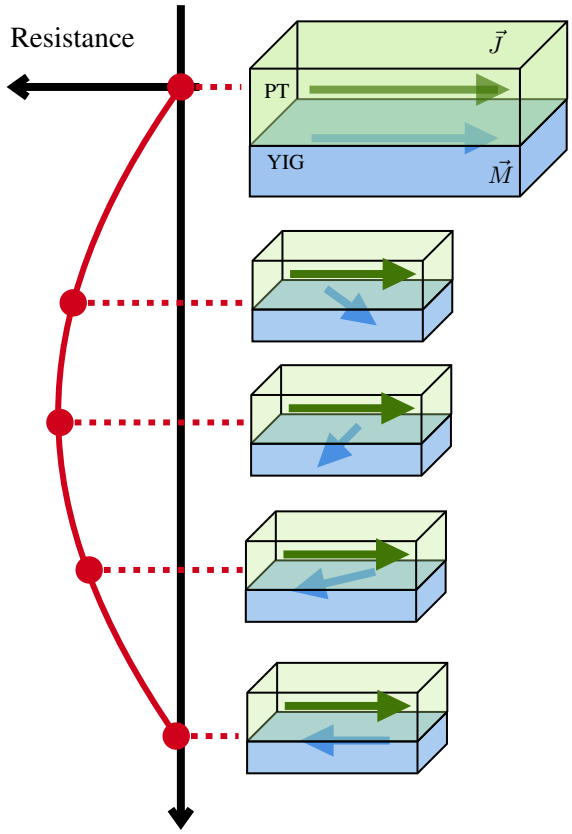

Figure 3: *Schematic representation of the Spin Hall Magnetoresistence [SMR]. The resistance of the conductor [Pt] is modulated by the magnetization direction of the insulating layer [YIG].*

Even though this analysis was consistent with previous reports form Wilhelm *et al.* [33] in which Pt develops an induced magnetization, the magnetoresistence [MR] was still observed when an additional copper [Cu] layer was deposited in between the ferrimagnet and the Pt layer [34]. Copper is not easily magnetized; thus, the explanation based on an induced magnetization seems unlikely. This motivated Chen *et al.* to suggest that this effect is a new type of magnetoresistence [30, 34, 35]. In their first 2013-paper [34], they argued that this new MR originates due to a non-equilibrium spin accumulation at the Pt|YIG interface and involves the simultaneous action of the spin Hall and inverse spin Hall effect (see Fig. 8).

Aqeel *et al.* [28] speculated that if the length-scales at which spin textures vary are much longer than the spin diffusion length, then the physical elements at the basis of the theory for SMR should still hold. Therefore, SMR could be use to electrically probe those textures. In 2016, the first experiment [28] employing SMR to detect spiral spin structures was published. Soon, other non-collinear magnetic orders were studied [36–42]. Surprisingly, some of the measurements [42] disclosed gaps in the current theoretical understanding of the SMR. For instance, new symmetry-allowed phenomenological terms —not predicted by Chen *et al.*— had to be introduced. To this day, the microscopic origin of these phenomenological terms is unclear. Thus, in order for SMR to further establish as a viable method to detect non-uniform magnetic textures, a comprehensive theoretical understanding of the effect is needed.

Overview

In this work, we discuss the theoretical assumption at the basis of the current theory for the SMR. We review the experimental results which employ this technique for detecting magnetic textures emphasizing the mismatch between theoretical predictions and measurements —whenever present. Finally, we compare this approach with other electrical detection techniques, and discuss its possible role in next-generation spintronics.

To that end, the necessary theoretical background and assumptions on which the main theory is built are introduced in section 2. We comment on the known limitations of the model based on previous theoretical investigations of the Spin Hall and Inverse Spin Hall Effects —quintessential elements in the current model. In section 3, we briefly describe some of the "exotic" magnetic orderings in ferrimagnetic crystals. We discuss the relevant physics that gives rise to those structures such as the Dzyaloshinskii–Moriya interactions [DMIs]. Additionally, we summarize the most widely used experimental techniques to observe these magnetic textures including novel electrical detection methods.

In section 4, we link the contents of section 2 and 3 by explaining how the signal generated by the SMR is able to give insight into the magnetic ordering. Additionally, we introduce the subsequent modifications made to the theory in order to explain the discrepancy between theoretical predictions and experimental measurements. We discuss some of the

[3] A dependence of the electrical conductance of a magnetic material on its magnetization direction [32].

theoretical weak points of the current SMR theory and speculate on how those points could be related to the theoretical modifications. Finally, we conclude the work with section 5 by shortly commenting on the perspectives that SMR has for next-generation spintronics and comparing and contrasting it with other all-electrical detection techniques.

2 Theoretical background

In this section we present the theoretical elements necessary for understanding the current theory [30, 34]. We introduce the relevant physical interactions that are evoked to describe the SMR. This include the Spin Hall Effect, the Inverse Spin Hall Effect, and the quantum mechanical boundary conditions (spin-mixing conductance). No previous knowledge of the field is assumed.

2.1 Hall Effects

Ordinary Hall Effect

When current flows through a **non-magnetic conducting material** [NM] in the presence of a perpendicular magnetic field, a voltage transverse to the direction of the current can be measured (see Fig. 4A). This effect is known as the **Ordinary Hall Effect** [OHE] and was discovered by Edwin Hall in 1880 [43, 44]. Today, it is a well-known and established phenomenon which has played a crucial role in the development of solid state physics and continues to be important for a variety of applications [45–47].

The effect is typically explained by treating the conductor as a sea of nearly-free charged carriers (Drude's model [45]). The presence of the magnetic field deflects the carriers' trajectories which then accumulate at the boundaries thus creating a measurable voltage difference (see Fig. 4B) [45, 48–50]. A relation between the transverse voltage (V_{H}), the longitudinal current (I_{long}), and the magnitude of the magnetic field (B) can be deduce by solving the carriers equation of motion[4] with the additional boundary condition that no current leaves the conductor in the transverse direction (i.e. $I_{\mathrm{trans}} = 0$)[5].

It is possible to prove that the transverse voltage (V_H) scales linearly with the longitudinal current (I_{long}) and the magnitude of the magnetic field (B) —for weak fields. This is expressed in Eq. 1. [51]. The proportionality constant (R_H) depends on the geometry of the material and on the mobilities and concentration of the carriers [51]. In fact, finding the proportionality constant via a series of transverse voltage *vs* magnetic field measurements has been a standard way of measuring (Hall) mobilities and carrier concentration in semiconducting materials [52].

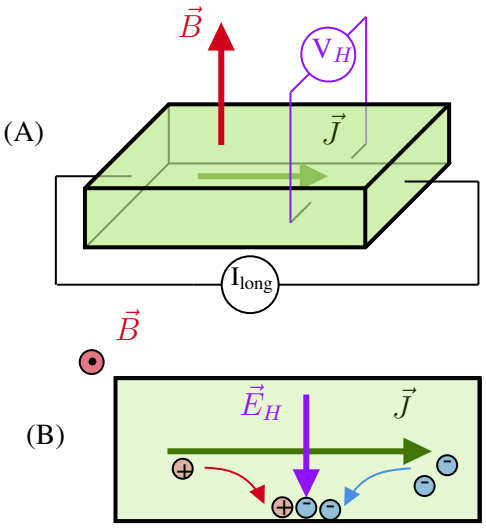

Figure 4: *(A) Schematic illustration of the Original Hall Effect [OHE]: a perpendicularly applied magnetic field $\vec{B}$ and a longitudinal current $\vec{J}$ generate a transverse voltage known as the Hall voltage (V_H). This voltage depends linearly on the intensity of the magnetic field. (B) Representation of charge carriers getting deflected by the magnetic field. At equilibrium, an electric field $\vec{E}_H$ perpendicular to $\vec{B}$ and $\vec{J}$ will be developed; this gives rise to the Hall voltage.*

$$\vec{E}_H = -R_H \left[\vec{J} \times \vec{B}\right] \implies V_H \propto B I_{\mathrm{long}} \tag{1}$$

It is interesting to note, that the relation between current density $\vec{J}$, electric $\vec{E}_H$ and magnetic field $\vec{B}$ stated in Eq. 1 is the only combination of these quantities —to first order in both— that is consistent with the full symmetries of the problem. Indeed, let us assume, that an electric field parallel to the magnetic field was present, say $\vec{E}_{\parallel}$. To first order, this field would have to satisfy Eq. 2, where $\vec{K}$ is

[4]The equation usually takes the form of Newton's law in the presence of the Lorentz force and an additional momentum-relaxation term arising from microscopic collisions. This last term is related to the carrier's (constant) mobilities for stationary solutions [45, 51]. An alternative approach involves solving Boltzmann's equation for the charge density.

[5]This condition can be replaced by the requirement that the nearly-free carriers experience no net force only in the case in which a single type of carrier is present. Both Ref. [48] and Ref. [49] present the no-net-force condition while Ref. [45] presents the more general boundary condition.

a constant vector determined by the geometry of the problem. By performing a mirror reflection through the plane perpendicular to $\vec{B}$, we can obtain: $\vec{B} \to \vec{B}$, $\vec{J} \to \vec{J}$, and $\vec{E}_{\parallel} \to -\vec{E}_{\parallel}$. These transformations follow from the fact that $\vec{B}$ is an axial vector, $\vec{J}$ lies in-plane, and $\vec{E}_{\parallel}$ is a polar vector [53]. Substituting those values in Eq. 2 gives Eq. 3. Both Eqs. 2 and 3 can be simultaneously satisfied only in the case when $\vec{E}_{\parallel}$ is identically zero, as was to be shown[6]. This small example illustrates the power of symmetry arguments in deducing functional relation. A similar technique will be employed in section 4.2.

$$\vec{E}_{\parallel} = \vec{B}\left[\vec{K}\cdot\vec{J}\right] \tag{2}$$

$$\underset{Mirror}{\Longrightarrow} (-\vec{E}_{\parallel}) = (+\vec{B})\left[\vec{K}\cdot(+\vec{J})\right] \tag{3}$$

Today, a whole zoo of Hall effects has been reported and although some bare little resemblance to the original effect described by Hall, they all can be described as some type of transverse response due to a longitudinal current [54]. For example, the OHE can be re-expressed as a longitudinal charge-current generating a transverse charge-accumulation as a result of the magnetic field deviation via the Lorentz force. Another example is the Spin Hall Effect [SHE]; this effect describes how a charge-current generates a transverse spin-accumulation. The description and the physical interactions that give rise to this effect are the topic of next section.

Spin Hall Effect

In 1928, Dirac introduced a new relativistically invariant quantum equation of motion for the electrons [55]. The equation incorporated spin as an intrinsic property of the particle, and predicted that its direction could be affected by the motion of the electron in the relativistic limit [56]. Mott [57] proposed that this relativistic effect would lead to spin-dependent scattering[7]; in other words, when an unpolarized beam of electrons (i.e. electrons without a preferential direction of their spin) interacts with a scattering center spin-up electrons will preferentially scatter in one direction —say the right— while spin down electrons will scatter in the opposite direction —left. This is illustrated in Fig. 5A.

Mott's asymmetric scattering was experimentally observed in the 50s [58]. This paved the way for Dyakonov and Perel [59] to theorized that a similar effect could occur due to impurities in a semiconductor crystal. The interactions would effectively "separate" a longitudinal current into spin up and spin down contributions at opposite ends of the semiconductor; therefore creating a transverse spin-polarized current. Since a non-magnetic material has equal number of spin up and down electrons, no net charge unbalance would be created. The effect was generalized to other types of materials and subsequently became known as the **Spin Hall Effect** [SHE]. This effect is illustrated in Fig. 5B. In analogy with the OHE, a longitudinal input creates a transverse response, but unlike the OHE, the SHE does not require an external magnetic field.

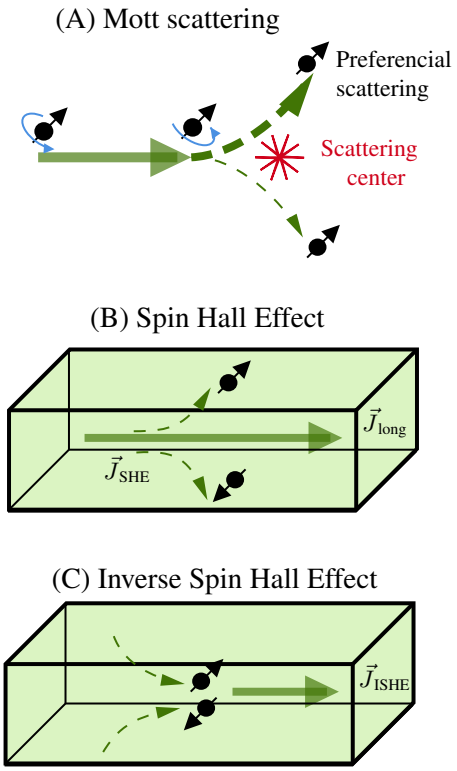

Figure 5: *(A) Schematic representation of Mott scattering. The electrons will preferentially scattered in the direction that "respect their spinning direction". (B) In the Spin Hall Effect [SHE], the spin-dependent scattering converts a charge current ($\vec{J}_{long}$) into a perpendicular spin current ($\vec{J}_{SHE}$); the spin-direction is perpendicular to these both charge and spin currents. (C) The spin currents can be recombined via the Inverse Hall Effect [ISHE] to create a new charge current ($\vec{J}_{ISHE}$).*

The first experimental investigation on the SHE [60] obtained results inconsistent with the theoretical

[6] A component of the electric field parallel to the current density is ruled out by performing a 2-fold rotation around the current direction, in this situation, only $\vec{B}$ would change sign.

[7] In lay terms, we can think that the electron spin interacts with the nucleus via spin-orbit coupling. This coupling is completely relativistic in origin.

predictions. Following studies, however, succeed in detecting the SHE signal [61] and now the effect is a standard procedure for measuring spin currents [54]. Most likely, the original experiments observed contradicting results due to inhomogeneous current injection and thus high levels of background noise created by the use of ohmic contacts as oppose to tunnel barriers [54]. This serves as a cautionary tale that transport experiments are particularly hard to interpret and often depend strongly on device quality.

The original theoretical description adopted by Dyakonov and Perel followed phenomenological grounds based on symmetry and drift-diffusion equations [54, 59]. In other words, they treated the spin currents and charged currents as classical fields obeying diffusion-like partial differential equations. Later on, Hirsch [62] and Zhang [63] realized that contributions completely intrinsic to the band structure could create spin-dependent scattering events. Zhang's work employed the semi-classical Boltzmann equation; this equation models the probability density function of thermodynamic variables near equilibrium, and thus, operates at a "more microscopical" approach than Dyakonov and Perel diffusion equations.

The connection of these intrinsic and extrinsic (Mott asymmetric scattering) effects and their contributions to the overall SHE and the related Anomalous Hall Effect [AHE][8] have already been thoroughly investigated in other review articles [54] and will not be included in this work. Suffice it to say, that the formalism based on the Boltzmann equation reduces to Dyakonov and Perel phenomenological equations in the limit of weak spin-orbit coupling. In the strong spin-orbit regime, the intrinsic contribution give rise to coherent effects[9] —completely quantum mechanical in nature— which are hard to incorporate into the diffusion equations. [54, 66].

Turning back to Dyakonov's and Perel's phenomenological description, it is surprising that all the complex microscopical processes and interactions (spin-orbit coupling, Berry curvature, band transport, etc.) can be reduced to a simple diffusion model employing elementary concepts of near-equilibrium thermodynamics as those introduced by Onsager and Prigogine [67–70]. The model correctly describes the SHE (in the weak limit) [66] — while completely disregarding its microscopic origin. This phenomenological approach has even been successfully applied to describe other effects within spintronics like in the emerging field of spin caloritronics [71]. In this framework, inhomogeneities of the intensive thermodynamic variables create fluxes of their conjugate variable. For example, an inhomogeneity in chemical potential will create a particle/mole current (Fick's law), an inhomogeneity in temperature will create a heat flux (Fourier's law) and so forth [67]. These fluxes are related to their conjugated variables via conservation/diffusion-like equations. Under the assumption that the system does not deviate significantly from its equilibrium state, and that memory effects can be ignored, a linear relationship between the gradients and the currents is justified.

In this approach the SHE is described by treating the polarized-electrons as different species of particles and allowing their chemical potentials to differ from the chemical potential solely due to charge. This is a mathematical trick, and no fundamental distinction between polarized and unpolarized electrons should be understood (they are still the same type of particles!). The difference between the spin-up(down) and charge chemical potential is referred to as the **spin accumulation**. The inhomogeneities of this spin density drive a spin-current via Onsager's linear relation, and the diffusion equations connect the spin-current with the charge current.

Onsager's relationship is symbolically expressed in Eq. 4. For simplicity, we have neglected the vector nature of this currents, the spin and charge current should be understood to be perpendicular to each other. In equation 4, j_e represents the charge-current, j_s represent the excess spin current, σ is the bulk electrical conductivity, μ_c is the charge chemical potential, μ_s is the spin accumulation (excess chemical potential due to spin), e is the electron charge, and θ_H is a dimensionless parameter called the **Hall angle**.

$$\begin{bmatrix} j_e \\ j_s \end{bmatrix} = \sigma \begin{bmatrix} 1 & \theta_H \\ \theta_H & 1 \end{bmatrix} \begin{bmatrix} -\nabla\mu_c/e \\ -\nabla\mu_s/(2e) \end{bmatrix} \tag{4}$$

The matrix of the response coefficients, which

[8] The AHE describes the appearance of a transverse charge accumulation in a magnetized conductor whenever a longitudinal charge current is present. Unlike in the OHE, the AHE does not require an external magnetic field. The extrinsic contribution to this effect arise from atoms with magnetic moments which scatter the charge carriers of the original longitudinal current. Similar to the SHE, intrinsic contributions due to the band structure are also present [64].

[9] In Quantum Mechanics, a carrier can be in a superposition of spin states. This does not hold classically thus interference effects cannot be reproduced. One example of a coherent effect is the collective spin procession of a spin current in the presence of a magnetic field known as the Hanle effect [65].

connects the fluxes with the gradients, is symmetric by virtue of Onsager's reciprocal relations (microscopic reversibility) [69, 70]. The diagonal terms capture Ohm's law of conduction, where the gradient of a chemical potential ($\nabla\mu_e$) is understood as an effective electromotive force or voltage (V_{eff}). The lower off-diagonal term relates how this voltage can create an excess spin current (j_s) and thus describe the SHE. The strength of this interaction is determined by the value of θ_H, where a higher value implies a more efficient conversion of charge current into spin current.

The Hall angle and the conductivity are intrinsic properties of each material and —in principle— depend on the intensive parameters of the system, such as temperature, pressure, and even chemical potential itself! At the phenomenological level, no further information can be given. In practice, θ_H also shows a dependence on the purity and the deposition technique used to create the devices [72]. Therefore, consensus on the true value of the Hall angle for each material is hard to achieve [54].

Nevertheless, some clear trends have been observed; for example, the magnitude of θ_H seems to scale with the fourth power of the nuclear charge (Z^4) [73]. This means that heavy 5d metals such as platinum [Pt] tend to display a larger SHE than 4d metals such as palladium [Pd] [54]. This is the reason why Pt in particular, is the go-to choice when making devices exhibiting the SHE. The Z^4 dependence also appears in the spin-orbit interaction [74] and thus corroborates the role of this effect in the SHE. Furthermore, the variations due to deposition techniques are consistent with the model that the (extrinsic) SHE arises due to Mott scattering in material defects.

Inverse Spin Hall Effect

Since the response matrix in Eq. 4 is invertible, it is possible to interpret this equation in an inverse but equivalent way. In this new interpretation, currents drive the gradients of chemical potential. Thus, a spin-current (j_s) can generate a gradient in the charge chemical potential (-$\nabla\mu_c/e$) which manifested as a voltage difference. This is illustrated in Fig. 5C.

The inverse Onsager relation is expressed symbolically in Eq. 5. The conversion of a spin-current into a voltage is determined by the upper off-diagonal elements. Just like in the SHE, this effect is dominated by the Hall angle (θ_H). Thus, the effect is more easily observed in 5d heavy metals.

$$\begin{bmatrix} -\nabla\mu_c/e \\ -\nabla\mu_s/(2e) \end{bmatrix} = \frac{1}{\sigma(\theta_H^2-1)} \begin{bmatrix} -1 & \theta_H \\ \theta_H & -1 \end{bmatrix} \begin{bmatrix} j_e \\ j_s \end{bmatrix} \quad (5)$$

The generation of a transverse voltage via a spin-currant has been observed experimentally [61] and today is known as the **Inverse Spin Hall Effect** [ISHE]. The usefulness of this phenomenon was quickly recognized by the spintronics community and now, ISHE-measurements have been established as a standard way of measuring spin-polarized currents [54].

Boundary Conditions

To complete the phenomenological description of the SHE, the diffusion/conservation equations must be added. This equations tend to be multi-dimensional partial differential equations, and as such require appropriate boundary conditions to be solved. To begin, we consider the simplest case in which a **non-magnetic/normal metal** [NM] has an interface with the vacuum [vac]. In that situation, no charges leave the conductor through the interface. Thus, the component of the current perpendicular to the surface must be zero [75]. This condition is identical to the one used in the derivation of the OHE.

The interfaces between a NM and **magnetic materials** [FM] (ferromagnets, ferrimagnets)[10] are more subtle and have been the topic of considerable theoretical investigations [75–78]. A comprehensive review of this topic can be found in Ref. [78]. The complication stems from the fact that the electron spin can interact with the local magnetic moments of the FM via exchange interactions, such as the Hund's rule coupling, allowing for spin mixing and even transfer of angular momentum to the FM [30, 76, 79].

A simple and extremely successful approach to model NM|FM interfaces is given by the **two-channel model** [78]. In this framework, the electrons are divided into majority carriers (electrons whose spin aligns with the magnetization direction) and minority carriers (their spin is anti-align). These two types of carriers move in different conduction channels within the materials and are allowed to have different probabilities of reflection and transmission at the interface (see Fig. 6A and 6B). Surprisingly, these elements are enough to explain effects such as the gigant magnetoresistence [GMR] and the tunnel magnetoresistence [TMR] [32, 80]. The former being the topic of the 2007 Nobel prize in Physics [81].

[10] The SMR has mainly been observed between a heavy metal (like Pt) and an insulating ferrimagnet. In the literature, however, there seems to be an implicit convention of ignoring the ferrimagnetic character and refer to this layer as a ferromagnet.

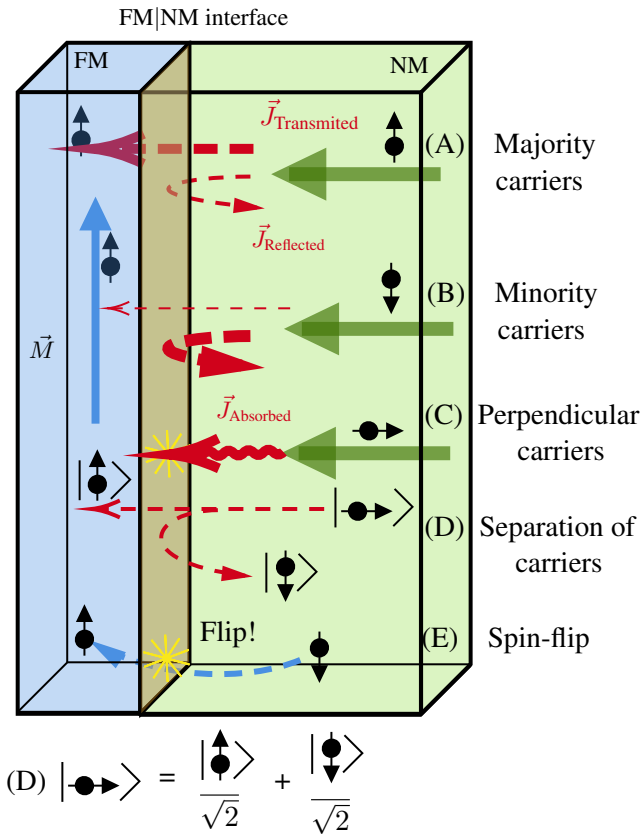

Figure 6: *Schematic illustration of different phenomena at the interface. In panel (A), electrons with the spin aligned in the same direction as the magnetization —majority carriers— tend to have a high probability of transmission. In panel (B), electrons with anti-align spins —minority carriers—, tend to be reflected. In panel (C), electrons with spin perpendicular to the magnetization will be absorbed by the FM and induce a torque. In (D), the perpendicular spin is expressed as a superposition of parallel and anti-parallel spins; the former is transmitted while the latter is reflected. This explains the disappearance/absorption of perpendicular carriers. In (E), the interface mediates a spin-flip.*

If we denote by $r_{nm}^{\uparrow(\downarrow)}$ the reflectance of majority (minority) carriers from channel n in the NM to channel m in the FM, we can define two **spin-dependent conductances** [30, 78]. These are given in Eq. 6, where h is Plank's constant and δ_{nm} is Kronecker's delta.

$$\begin{aligned} G^{\uparrow} &= \tfrac{e^2}{h}\textstyle\sum_{nm}\left[\delta_{nm} - |r_{nm}^{\uparrow}|^2\right] \\ G^{\downarrow} &= \tfrac{e^2}{h}\textstyle\sum_{nm}\left[\delta_{nm} - |r_{nm}^{\downarrow}|^2\right] \end{aligned} \tag{6}$$

As discuss previously, inhomogeneities in the charge and spin chemical potentials drive current of these quantities (diagonal terms in Eq. 4). In the two-channel model, an analogous condition holds at the boundary —where discontinuities play the role of the inhomogeneities. If we denote by $\mu_c^{NM(FM)}$ the charge chemical potential at the interface of the NM (FM), a current of majority ($j^{\uparrow}$) (minority ($j^{\downarrow}$)) carriers will flow according to Eq. 7. Interpreting the chemical potentials as an effective voltage, Eq. 7 has the form of the familiar Ohm's law.

$$\begin{aligned} ej^{\uparrow}|_{\text{charge}} &= G^{\uparrow}\left[\mu_c^{NM} - \mu_c^{FM}\right] \\ ej^{\downarrow}|_{\text{charge}} &= G^{\downarrow}\left[\mu_c^{NM} - \mu_c^{FM}\right] \end{aligned} \tag{7}$$

Discontinuities in μ_s will also drive currents of majority/minority carriers. However, the full vector nature of the electron spin must be taken into account. We introduce the quantity $\vec{\mu}_s = (\mu_{s_x}, \mu_{s_y}, \mu_{s_z})$, where μ_{s_i} is the spin-chemical potential of carriers with spin in the i-direction. Since we are treating electrons as either align or anti-align to the magnetization, only the component of $\vec{\mu}_s$ parallel to the FM's magnetization will induce a current of the carriers in a similar fashion as the discontinuities in μ_c. Mathematically, this is expressed in Eq. 8, where $\hat{m}$ is a unit vector in the direction of the FM's magnetization, and μ_s^{FM} is the spin chemical potential in the ferromagnet. The vector character of μ_s^{FM} is not taken into account, since the strong exchange interactions will tend to align (anti-align) all carriers, thus the perpendicular component of μ_s^{FM} is negligible.

$$\begin{aligned} ej^{\uparrow}|_{\parallel} &= G^{\uparrow}\left[(\vec{\mu}_s^{NM})\cdot(\hat{m}) - \mu_s^{FM}\right] \\ ej^{\downarrow}|_{\parallel} &= G^{\downarrow}\left[(\vec{\mu}_s^{NM})\cdot(\hat{m}) - \mu_s^{FM}\right] \end{aligned} \tag{8}$$

To account for spin-accumulation orthogonal to the magnetization direction, the two-channel model appeals to the notion that a carrier with a perpendicular spin can be described as a superposition of an align and an anti-align state (see Fig. 6D). The align contribution enters into the FM while the anti-align is reflected back into the NM. The parallel spin current is conserved in this interaction[11], while the perpendicular current is not. This can be summarized in the rule-of-thumb: "perpendicular currents get absorbed" (see Fig. 6C) [78]. To model the interconversion of perpendicular current into parallel current, a **spin-mixing conductance** ($G^{\uparrow\downarrow}$) is introduced [78]. This is given in Eq. 9, were $*$ denotes the complex conjugate. It is worth remarking that this conductance will, in general, be a complex number, and thus we can separate it into its real (G_r) and imaginary part (G_i).

[11] The total parallel current at the beginning is zero. At the end, equal and opposite parallel contributions are created.

$$G^{\uparrow\downarrow} = G_r + iG_i = \frac{e^2}{h}\sum_{nm}\left[\delta_{nm} - (r^{\uparrow}_{nm})(r^{\downarrow}_{nm})^*\right] \tag{9}$$

Due to the conservation of angular momentum, the absorbed perpendicular current must induce a torque in the FM. The two-channel model usually describes this torque by means of the phenomenological Landau–Lifshitz–Gilbert-Slonczewski equation [LLGS][12], where the spin-accumulation plays the role of an effective magnetic field [78, 82]. The rate of change of the magnetization will generate an electromotive force (Faraday's law) which can be related to the spin current via the spin-mixing conductance (Ohm's law).

The contribution of the orthogonal components of the spin accumulation to the spin current are expressed in Eq. 10. The vector character of the spin is now taken into account, here $\vec{j}_s = (j_{s_x}, j_{s_y}, j_{s_z})$; in other words, the components of the vector $\vec{j}_s$ represent spin direction, not flow directions[13]. We also note that G_r is related to the procession of the magnetization while G_i is related to its damping. First-principle calculations have shown that for the majority of cases of interest $G_i \ll G_r$ [77, 78, 83] and thus, the first term in Eq. 10 tends to dominate the interaction.

$$\vec{j}_s|_{\perp} = -G_r\left[\hat{m}\times(\hat{m}\times\vec{\mu}_s^{NM})\right] - G_i\left[\hat{m}\times\vec{\mu}_s^{NM}\right] \tag{10}$$

Combining equations 7, 8, and 10, we obtain the most general boundary condition used in the two channel model [77, 78]. This condition is summarized in Eq. 11. Now, the charge and parallel contribution of the current include the term $\hat{m}$ to indicate that the spin is align with the magnetization direction; moreover, the spin current is shown to arise from the asymmetry between the currents of the two types of carriers (up minus down).

$$\vec{j}_s^{NM\to FM} = (j^{\uparrow}|_{\text{charge}} + j^{\uparrow}|_{\parallel} - j^{\downarrow}|_{\text{charge}} - j^{\downarrow}|_{\parallel})\hat{m} + \vec{j}_s|_{\perp} \tag{11}$$

In our discussion so far, no direct appearance of spin flipping (see Fig. 6E) was taken into account. The standard methods used in the fabrication of these heterostructures —DC-sputtering or E-beam deposition— create samples that are significantly different from perfect epitaxialy-grown crystals; in other words, the samples are said to be "dirty". This implies that discontinuities in the band structure between the FM and the NM occur at atomic scales [78]. First-principle calculations have reveal that interfacial spin flipping and scattering tend to dominate the properties of devices [84]. Nevertheless, these effects can be included in Eq. 11 by replacing the spin conductances defined in Eqs. 6 and 9 by effective values of these quantities [85]. Indeed, scattering theory has be used to theoretically predict these conductance even when disorder is taken into account without the need to introduce more free parameters [86].

2.2 Spin Hall Magnetoresistence

With all of the required theoretical background introduced, we present the model put forward by Chen *et al.* [30, 34] for SMR. We aim to follow their derivation as close as possible.

The system under investigation is a bilayer structure of a NM on top of an insulating FM (see Fig. 7). Without loss of generality, the z-direction will be chosen parallel to the normal at the interface and the longitudinal current will flow in the x-direction. Furthermore, the medium is assumed to be isotropic and homogeneous in the xy-plane, i.e. the equations and boundary conditions must be invariant under in-plane rotations and translations. The layers are assumed to be infinite in the x and y direction, the insulating FM also extends to minus infinity in the z-direction.

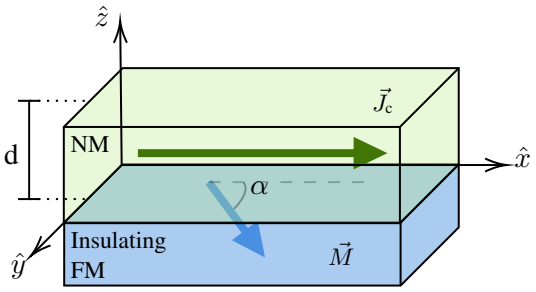

Figure 7: *Bilayer heterostructure used to theoretically model the SMR. The figure shows the labeling convention used in this work. The angle α lies in the xy-plane.*

The theory builds upon the phenomenological drift-diffusion equations employed to describe the SHE (see section 2.1). The spin current is described by a rank-2 tensor $j_{s_{kl}}$, where the index k indicates the

[12] This equation describes the evolution of the magnetization with time as a function of applied torques. It includes some well-known terms like the giromagnetic procession around and external field.

[13] The flow direction is given by the normal direction to the interface.

direction of the current, and the index l indicates the direction of the spin[14]. To simplify notation, we introduce $\vec{j}_{s_x} = (j_{s_{xx}}, j_{s_{yx}}, j_{s_{zx}})$ —the current of x-polarized electrons. Similar notation will be used for y and z spin directions. In addition, we denote the spin components to the flow in the k-direction as $\vec{j}_s^k = (j_{s_{kx}}, j_{s_{ky}}, j_{s_{kz}})$.

Following the discussion of section 2.1, we express Onsager's linear relation in Eq. 12. The response matrix $[L]$ is given given by Eq. 13, where $\hat{x}$ represents the Cartesian unit vector in the x-direction (and similar for $\hat{y}$ and $\hat{z}$). In accordance to equation 4, the matrix is symmetric owing to microscopic reversibility and the absence of an external magnetic field. The diagonal terms give Ohm's law and the lower-off-diagonal terms represent the SHE. It is worth noticing that the vector nature of the current, spin and transverse response is taken into account via the cross product ($\times$). As a rule of thumb, it is useful to keep in mind that the charge current direction, the direction of the spin-current, and the direction of the spin form a right-handed orthogonal basis. Finally, the zero elements in the matrix assume that the excess spin can only create currents of the same spin (no mixed spin contribution). First-principles calculations have shown that this assumptions holds true for cubic systems. However, anisotropic effects can be present in other crystalline systems, such as hexagonal closed packed lattices [87].

$$\begin{bmatrix} \vec{j}_e \\ \vec{j}_{s_x} \\ \vec{j}_{s_y} \\ \vec{j}_{s_x} \end{bmatrix} = \sigma[L] \begin{bmatrix} -\nabla\mu_c/e \\ -\nabla\mu_{s_x}/(2e) \\ -\nabla\mu_{s_y}/(2e) \\ -\nabla\mu_{s_z}/(2e) \end{bmatrix} \tag{12}$$

$$[L] = \begin{bmatrix} 1 & \theta_H\hat{x}\times & \theta_H\hat{y}\times & \theta_H\hat{z}\times \\ \theta_H\hat{x}\times & 1 & 0 & 0 \\ \theta_H\hat{y}\times & 0 & 1 & 0 \\ \theta_H\hat{z}\times & 0 & 0 & 1 \end{bmatrix} \tag{13}$$

Under steady-state conditions, the chemical potential inside the NM is assumed to satisfy Eq. 14. This equation was first postulated by Johnson *et. al.* [88, 89] and independently by van Son *et al.* [90] on purely phenomenological grounds. It differs from the usual steady-state diffusion equation by the addition of an extra term proportional to the chemical potential. This term originates from the spin-relaxation and spin-flipping and tends to drive the spin-excess chemical potential to zero. Valet and Fert [91] showed that in the limit when the spin diffusion length (λ) is much bigger than the electron mean free path, the Boltzmann equation agrees with Eq. 14.

$$\nabla^2\vec{\mu}_s = +\frac{\vec{\mu}_s}{\lambda^2}, \tag{14}$$

The solutions of Eq. 14 under the assumption of x and y transnational invariance are given by Eq. 15, where $\vec{A}$ and $\vec{B}$ are constants to be determined by the boundary conditions. In the bilayer structure, one of the interfaces of the NM is exposed to vacuum, while the other satisfies the boundary conditions for an insulating FM.

$$\vec{\mu_s} = \vec{A}e^{-z/\lambda} + \vec{B}e^{+z/\lambda} \tag{15}$$

As previously discussed, at the vacuum interface the components of the currents perpendicular to the surface must vanish. In our structure, $\hat{z}$ is the normal vector to the vacuum interface. Therefore all the flows in the z-direction must vanish. These conditions are given by Eq. 16, where the second equality captures the fact that no spin direction flows outside the NM.

$$\vec{j}_e \cdot \hat{z} = 0 \qquad \vec{j}_s^z\Big|_{\text{vac}} = \vec{0} \tag{16}$$

For the FM interface, Eq. 11 must be modified to account for the insulating properties of this layer. Under the assumption of a perfect insulator, the reflection coefficient must be equal to unity for either type of carriers ($|r_n^{\uparrow(\downarrow)}m|^2 = 1$) [30, 78][15]. This conditions implies that the spin-dependent conductances are identically zero ($G^\uparrow = G^\downarrow = 0$), but a non-zero spin-mixing conductance is possible as can be seen from Eq. 17.

$$|r_{nm}^{\uparrow(\downarrow)}|^2 = 1 \implies r_{nm}^{\uparrow(\downarrow)} = e^{i\phi_{nm}^{\uparrow(\downarrow)}} \tag{17}$$

$$\implies G_r + iG_i \propto \sum_{nm}\delta_{nm} - e^{i(\phi_{nm}^\uparrow - \phi_{nm}^\downarrow)} \neq 0$$

Therefore, only the perpendicular component of the interface current remains (see Eq. 10). The boundary condition at the FM is given by Eq. 18, where the minus sign appears because the normal at the FM interface is $-\hat{z}$ [30].

[14] For example, the component $j_{s_{xy}}$ answers the question: How many electrons are traveling in the x-direction with spin aligned in the y-direction per unit area per unit time?

[15] In essence, we are not allowing either spin up or down to travel inside the insulator

$$-\vec{j}_s^z(\hat{m})\Big|_{\text{FM}} = G_r\hat{m}\times(\hat{m}\times\vec{\mu}_s)+G_i(\hat{m}\times\vec{\mu}_s) \quad (18)$$

Combining equations 12, 15, 16, and 18 with the additional assumption that the charge chemical potential (μ_c) scales linearly with x (this models the original voltage difference that creates the longitudinal charge current), one can obtain a unique solution of the problem. The algebraic manipulation of the equations is cumbersome and non-trivial; for example, the boundary condition in Eq. 18 effectively relates the spin-current to the spin accumulation, while Eq. 12 relates the same current with the gradient of the spin accumulation.

Nevertheless, the main result for SMR can still be presented in an easy-to-use expression. The modulation of the resistance (ρ) of the NM by the magnetization direction of the insulating FM is given in Eq. 19, where the transverse resistance (ρ_{trans}) is defined as the ratio between the transverse current ($\vec{j}_e\cdot\hat{y}$) and the **longitudinal** voltage (parallel to $\hat{x}$), m_i is the component of the unit magnetization in the i-direction[16].

$$\begin{aligned}\rho_{\text{long}} &= \rho+\Delta\rho_0+\Delta\rho_1(m_x^2+m_z^2)\\ \rho_{\text{trans}} &= \Delta\rho_1(m_xm_y)+\Delta\rho_2(m_z)\end{aligned} \quad (19)$$

In their original paper, Chen *et al.* [34] give the approximate expressions for $\Delta\rho_0$, $\Delta\rho_1$, and $\Delta\rho_2$ in terms of the spin-diffusion length λ, the Hall angle θ_H, the spin-conductance G_r+iG_i, and the thickness of the NM layer. In general, all of the $\Delta\rho$ terms scale quadratically with the Hall angle (θ_H). Additionally, even though the final expressions for $\Delta\rho$ in Chen's *et al.* paper are approximate, the functional dependence with the magnetization components is not affected by their approximation. Just as in the discussion of the OHE (see section 2.1), symmetry arguments can be used to prove that Eq. 19 is the most general form —to second order in magnetization— consistent with the symmetries of the problem [42].

We can describe the conclusions of this theory in a more intuitive way. To that end, we shall assume that the magnetization lies in-plane ($m_z = 0$). The external electric current creates a transverse spin current due to the SHE. When the spin current reaches the insulating FM interface, two limit scenarios are possible. If the magnetization is parallel to the current direction ($m_x = 1$), the longitudinal resistance increases (ρ_{long} depends quadratically on m_x). This can be understood as the FM absorbing the incoming spin current. Indeed, in this scenario, the direction of the spins in the SHE-current is perpendicular to the magnetization (i.e. they are in the y direction) and can be absorbed by the FM, as was discussed in section 2.1 (see Fig. 8A).

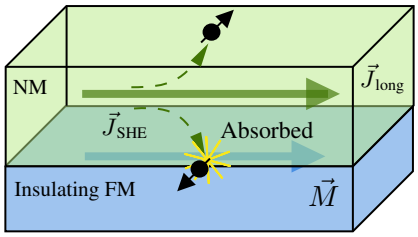

(A) High resistance

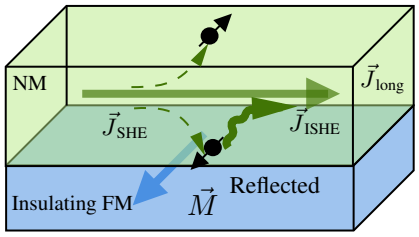

(B) Low resitance

Figure 8: *(A) When the current direction and the magnetization are parallel, the spin of the electrons generated by the SHE is orthogonal to the magnetization; thus, it will get absorbed at the surface. (B) If the current direction and the magnetization are perpendicular, the spin of the carriers will be collinear with the magnetization. Since the carriers cannot penetrate into the insulator, they will get reflected at the interface and later recombine via the ISHE to create an additional charge current, thus lowering the resistance.*

The second scenario involves a magnetization perpendicular to the current direction ($m_x = 0$), in which case the resistance decreases. This can be explained by a reflection of the incoming spin-current at the boundary between the NM and the FM. Indeed, in this case, the magnetization and the spin direction are parallel, and because of the insulating properties of the FM no currents are allowed to propagate. Subsequently, the reflected spin-current is recombined via the ISHE into the main longitudinal current increasing its value for any given longitudinal voltage. This extra contribution to the current will act as an effective reduction of the resistance. This is illustrated schematically in Fig 8B.

When the magnetization direction is in-between those states, both scenarios will happen simultaneously. This explanation also gives insight into why the

[16] One must keep in mind that z indicates the out-of-plane component and x the direction of the longitudinal charge current.

coefficients in Eq. 19 depend quadratically on the Hall angle: the SMR involves the action of both the SHE and the ISHE. In summary, the theory describes the SMR as a non-equilibrium process (using the diffussion/near-equillibrium thermodynamic models) in which a spin accumulation $\vec{\mu_s}|_{FM} \neq \vec{0}$ occurs at the interface, with the simultaneous action of the Spin Hall and Inverse Spin Hall Effects.

Experimental studies

Ever since the first SMR signal was inadvertently detected by Weiler *et al.* in 2012 [29], multiple experiments have been performed exploring the physical consequences of this magnetoresistence. In what follows, we will describe some of the most relevant results for non-uniform magnetization. The list is not —by any means— an exhaustive one and the interest reader is referred to Ref. [30] for more information.

The original explanation proposed by Weiler *et al.* [29] and Huang *et al.* [31] claims that the signal originates from the standard AMR displayed by a magnetized Pt layer. The Pt would be magnetize due to proximity effects by the already magnetized YIG. This is analogous to the induced magnetization observed in Pt|Ni bilayers as reported by Wilhelm *et al.* [33]. The dependence of the resistance on magnetization direction given by the AMR satisfies Eq. 20 [30], a simple inspection reveals that both Eq. 19 and Eq. 20 have the same phenomenological dependence for a completely in-plane magnetization ($m_z = 0$). Therefore, the models are indistinguishable for these sort of measurements, which was exactly the configuration used by Weiler *et al.* and Huang *et al.*.

$$\rho_{\text{long}}^{AMR} = \rho + \Delta\rho_0^{AMR}(m_x^2) \qquad (20)$$
$$\rho_{\text{trans}}^{AMR} = \Delta\rho_1^{AMR}(m_x m_y)$$

To settle this issue, Nakayama *et al.* [35] study the MR displayed by a Pt|Cu|YIG heterostructure. Copper, is not easily magnetized but has a considerable spin-diffusion length (hundreds of nm). Therefore, if the effect truly arises due to proximity effects, the copper layer should make the signal vanish. Their measurements showed the presence of a MR even when a 12nm layer of Cu was introduced, thus ruling out the possibility of an induced magnetization in the Pt layer.

Vlietstra *et al.* [92] carried out experiments to determine the MR dependence for out-of-plane magnetizations, their results are in agreement with Eq. 19 corroborating the role of the SMR. In addition, they tried to use the functional expression for $\Delta\rho_0$, $\Delta\rho_1$, $\Delta\rho_2$ in Eq. 19 as a way to determine parameters such as G_i or θ_H, both of which are particularly hard to measure —as discussed in section 2.1 and 2.1. Their experiment consisted in measuring both longitudinal and transverse resistance of a Pt|YIG bilayer as a function of magnetic field direction. Subsequently, a fitting procedure was carried to determine the unknown parameters. Unfortunately, the results were not promising since the parameters in Eq. 19 are strongly correlated during the fitting procedures.

Vlieststra *et al.* [93] also studied the dependence of the SMR with Pt thickness. Their result show that the signal is stronger at smaller thickness which is consistent with the description of the simultaneous action of the SHE and ISHE. This can be rationalized as follows: at larger thickness, the reflection of the SHE spin-current in both the vacuum and FM interface cannot occur due to losses of spin polarization therefore diminishing the contribution of the ISHE and thus the reduction of resistance. They additionally investigated the dependence of the signal with deposition method. The signal for a device fabricated using DC-sputtering was orders of magnitude stronger than the one fabricated using E-beam evaporation. Sputtering is known to create more uniform depositions than E-beam and thus, their findings further stress the relevance of interface quality on magneto-transport experiments.

To conclude this section, it is worth mentioning that although the original investigations of the SMR were almost exclusively carried out in Pt|YIG bilayer [29, 31, 34, 35, 92, 93], the effect has now been reported for a variety of metals and insulators pairs such as: Pt|Fe_3O_4 [94], Pt|$CoFe_2O_4$ [95], Au|YIG [96], and may others [30]. Moreover, SMR has been the topic of a recent patent filed by Saitoh E., Nakayama H., and Harii K. for an electrical detection of an insulator magnetization using SMR [97].

3 Magnetic Ordering

In this section we briefly introduce the theoretical background to describe non-collinear magnetic orders and the microscopic and macroscopic interactions that give rise to them. Furthermore, we shortly comment on the techniques commonly used for their detection.

3.1 Magnetic phase diagrams

Its is well-known that classical physics —if applied consistently— predicts no permanent magnetization at thermal equilibrium[17] [98]. Therefore, a quantum mechanical approach to magnetic condensed matter seems unavoidable. This would entail the study of a highly non-trivial hamiltonian operator accounting for the interactions of the various atomic magnetic moments inside the the crystal.

In this regard, Landau and Lifshitz made a monumental contribution to Physics by introducing their theory of phase transitions [99]. This theory considerably simplified the complexity of the problem and makes theoretical studies possible. In this framework, the individual atomic magnetization inside a crystal are replaced by a continuous (vector) field $\vec{M}(\vec{r})$ which accounts for the magnetization density; this field also receives the name of the **order parameter**. The dynamics of the system are determined by the free energy density which takes the form of a functional[18] of the order parameter [100].

The fundamental assumption of Landau and Lifshitz is that the functional $(\beta\mathcal{H})$[19] can be expressed as a power series of the order parameter in which all terms consistent with the symmetry of the system must be included. A typical example of this free energy functional is given in Eq. 21 [101], where full-rotation and inversion symmetry are assumed. Coefficients t,u,k, etc., are phenomenological functions of the intensive parameters of the systems such as temperature, pressure, external magnetic field, etc. In the saddle point approximation [100, 101], the different phases and their transition are explored by solving the (field) Euler-Lagrange equation of a given functional.

$$(\beta\mathcal{H})_{\left[\vec{M}(\vec{r})\right]} = \int_{\mathbf{R}^3} \frac{t}{2}\left(\vec{M}\cdot\vec{M}\right) + u|\vec{M}|^4 + \frac{k}{2}\left(\vec{\nabla}\vec{M}:\vec{\nabla}\vec{M}\right) + ... \tag{21}$$

In 1958, Dilashenskii studied the ferrimagnetism ("weak" ferromagnetism) displayed by crystals such as α-Fe_2O_3, $MnCO_3$, and $CoCO_3$ [102] using Landau and Lifshitz formalism. To that end, he introduced new phenomenological terms to the free energy functional consistent with a cubic crystalline systems without inversion symmetry. His addition is summarized in Eq. 22, where D is the phenomenological constant related to Dilashenskii's new term, and $\vec{B}$ represents the coupling of the magnetization with an external magnetic field [22].

$$\text{DMI}: (\beta\mathcal{H})_{\left[\vec{M}(\vec{r})\right]} = \int_{\mathbf{R}^3} \frac{k}{2}\left(\vec{\nabla}\vec{M}:\vec{\nabla}\vec{M}\right) + D\vec{M}\cdot\left(\vec{\nabla}\times\vec{M}\right) - \vec{B}\cdot\vec{M} + ... \tag{22}$$

At the time, only the microscopical Heisenberg interaction between atomic magnetic dipoles was known. This interaction is expressed in Eq. 23, where $\hat{H}$ is the hamilton operator, $\hat{\vec{S}}_i$ is the spin (vector) operator at site i, and $J_{i,j}$ is a coupling constant between sites i and j [103]. The presence of the dot product $(\cdot)$ between the two spin operators grants full-rotation and inversion symmetry. Thus, Heisenberg interaction cannot account for Dilashenskii's term.

$$\hat{H}_{\text{Heisenberg}} = \sum_{i,j} J_{i,j}\left(\hat{\vec{S}}_i\cdot\hat{\vec{S}}_j\right) \tag{23}$$

By including relativistic effects, such as the spin-orbit coupling between the different lattice sites, Moriya showed that new anti-symmetric interactions appear in the hamiltonian. These interactions are given by Eq. 24, where now the coupling between site i and j is governed by the vector $\vec{D}_{i,j}$ [104]. The presence of the cross product breaks inversion symmetry and the crystal system is taken into account by the functional form of the coupling vector[20]. This interaction recovers the term proportional to the curl in Eq. 22 in the continuous limit for a cubic crystal system [105].

$$\hat{H}_{\text{DMI}} = \sum_{i,j} \vec{D}_{i,j}\cdot\left(\hat{\vec{S}}_i\times\hat{\vec{S}}_j\right) \tag{24}$$

Today, the hamiltonian expressed in Eq. 24 and the term proportional to the curl in Eq. 22 are known as the **Dilashenskii-Morija interactions** [DMI] or **anti-symmetric exchange**, their inclusion to the (free) energy had unexpected consequences for the ground

[17] This is known as the Bohr–Van Leeuwen theorem.

[18] A functional is a function that takes a field as is input (the field can be a vector field or a scalar field) and returns a real number. In general, the functional can depend on properties of the input field such as its derivatives. If the interactions are assumed to be local, the functional can be expressed in an integral form.

[19] In Eq. 21, $(\beta\mathcal{H})$ must be understood as a single symbol. The choice is historical and is made to resemble the notation used in Statistical Physics to calculate partition functions [68, 101]. We are following the convention $\overleftrightarrow{a}:\overleftrightarrow{c} = \sum_{i,j}(\overleftrightarrow{a})_{i,j}(\overleftrightarrow{c})_{i,j}$.

[20] Under inversion neither of the spin operators change sign since angular momentum has even parity, but the right handed system turns into a left handed system, and thus the cross product must change sign. If $\vec{D}_{i,j}$ also has even parity, the entire interaction changes sign under inversion and thus is anti-symmetric.

state of magnetic materials. Indeed, the Euler-Lagrange equations of the functional in Eq. 22 predict that —for certain values of the phenomenological coefficients k,D,$\vec{B}$,etc.— the state of minimum (free) energy is given by a non-uniform magnetization, such as helices, cones[105], skyrmions [22, 106], etc. (See Fig. 9 and Fig. 2).

Because the phenomenological coefficients are analytic functions of the intensive parameters, the same crystal can exhibit different magnetic arrangements depending on its temperature, pressure, external magnetic field, etc. To capture this scenario, a magnetic phase diagram is employed (see Fig. 9). In these diagrams, the axis label the intensive parameters and regions inside the diagram are colored according to which magnetic texture the crystal exhibits. This situation is not unlike the phase diagrams typically shown for paramagnetic-ferromagnetic [103]. The boundary between these regions represents a phase transition, and for a fixed temperature T, it usually occurs at a critical value of the external field $B_c(T)$.

3.2 Skyrmions

From all the previously discussed non-uniform phases, the skyrmionic phase (A-phase in Fig. 9) has attracted the most attention from the spintronics community [19, 22, 23]. This phase is populated by multiple skyrmions and was originally theorized by Bogdanov and Yablonskii in 1989 [106]. Each individual skyrmions —which receives its name from the pioneering work of Skyrme [107]— is a spin arrangement that cannot be continuously deformed into a uniform magnetic state (see Fig. 2A)[21] [22]. This defining property grants skyrmions particle-like properties such as a size (typically 5 to 100nm)[22] [22], and the ability to move under the application of electrical currents [108]. Today, it is understood that other mechanisms besides DMI can give rise to skyrmions [22], some examples include frustrated exchange interactions [109] and four-spin exchange interactions [110].

The presence of skyrmions is not limited to their equilibrium region in the magnetic phase diagram. Indeed, researchers have found that these quasi-particles can exist in a metastable state for a considerable range of temperature and applied magnetic field. These metastable regions have been reported in crystals, such as $Fe_{1-x}Co_xSi$ [111], $Co_8Zn_8Mn_4$ [112], MnSi [23], and Cu_2OSeO_3 [113]. The latter —copper oxide selenite [CSO]— stands out since it displays a tilted conical phase and two stable skyrmionic phases: one at low temperature (near the field-polarized region) and one at high temperature (near the paramagnetic region) [113].

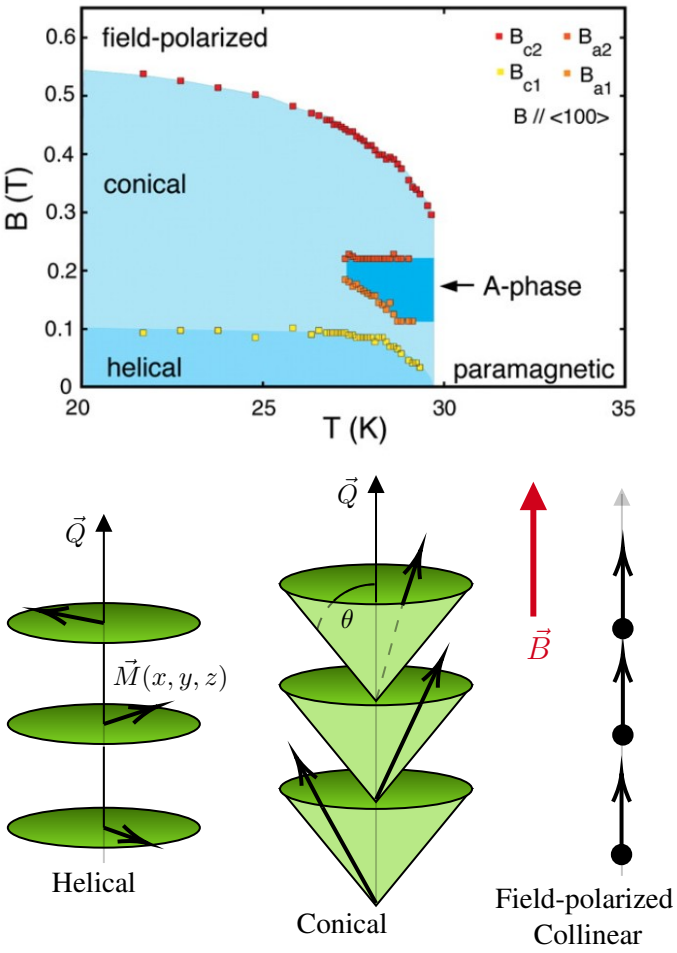

Figure 9: *Examples of Magnetic phases. The textures are displayed by the crystal of manganese monosilicide [MnSi]. A-phase is the skyrmionic phase. Phase diagram taken from [24]. Spin drawings by the authors.*

All of these properties have lead some scientist to propose skyrmions as possible information carriers for ultra-dense memory applications [19, 23]. This vision, called **skyrmionics**[23], is not without its challenges. Theoretical investigations have shown that in the presence of boundaries or other crystal defects, the energy barrier for the transition between a skyrmion and an uniform magnetization —which in bulk materials is dominated by the topological protection— is severely diminished. Moreover, its

[21] Different types of skyrmions exist according to their topological properties, such as vorticity and helicity. The mathematical definition of these parameters is outside the scope of the present work.

[22] These skyrmions, however, are typically around 1nm in size and cannot be studied using the continuum description of section 3.1.

[23] Skyrmions + electronics = skyrmionics.

magnitude is such that at room temperature thermal fluctuations can easily surpass it [114]. Even so, researchers remain optimistic that studies into device material and design will be able to address those difficulties [23].

In spite of all of its challenges, skyrmionics continues to be a promising field of research and has achieved impressive milestones. Indeed, on March 2022, Wang *et al.* [115] successfully demonstrated that nanosecond electrical pulses are able to create, delete, and deterministically transport skyrmions through a $Co_8Zn_{10}Mn_2$ magnet at room temperature. Nevertheless, Wang's *et al.* experiment still relayed on LTEM measurements to visualize these quasi-particles, making their device far from a stand-alone all-electrical component.

3.3 Experimental techniques

The first experimental observations of non-uniform magnetic textures, such as helices or cones (see section 3.1), were carried out in the 70s [116]. The skyrmionic phase, however, was not experimentally verified until 2009, when neutron scattering experiments confirmed its presence in MnSi magnets [24, 117, 118]. Currently, two main technique for the detection of skyrmions are used: neutron scattering for reciprocal-space imaging and LTEM for real-space images [22].

Neutrons posses an intrinsic magnetic moment which allows them to probe magnetic arrays within a crystal. In scattering experiments, the neutron wavefunction constructive interference whenever the Bragg's condition is satisfied. This condition is stated in Eq. 25, where λ_n is the neutron wavelength, d_n is the effective distance between parallel crystal planes, and θ is the scattering angle. The situation is similar to conventional X-ray diffraction experiments[24] with the important difference that now the periodicity will take into account the magnetic order of the crystal [120]; thus, d_n is considerably bigger than the crystal lattice constant. As a consequence, the diffraction condition can only be satisfied for small angles. Indeed, in section 3.1 we mentioned that DMI give rise to skyrmions in the order of 5-100nm. In neutron scattering experiments λ_n ranges from 0.04-3nm [120]. This implies $d_n \gg \lambda_n \implies \sin(\theta) \ll 1$. Which explains the small angle requirements. Therefore, the observation of skyrmions in reciprocal space involves **small angle neutron scattering** [SANS] measurements [22, 24].

$$\sin(\theta) = \frac{\lambda_n}{2d_n} \tag{25}$$

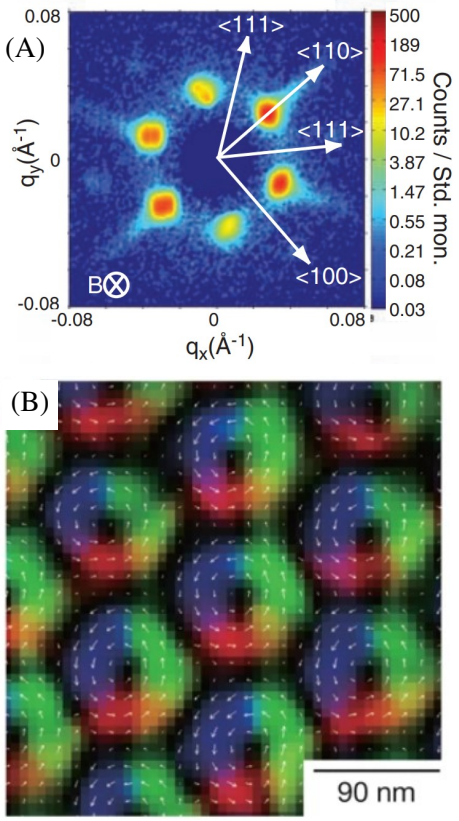

Figure 10: *(A) Reciprocal-space image using SANS of the skyrmionic phase. The skyrmions arrange in a honeycomb structure as can be seen in the real-space image (B) taken with LTEM measurements. This explains the appearance of a hexagon in the diffraction pattern (the Fourier transform of the honeycomb lattice is a rotated honeycomb lattice). Image (A) taken from [24], image (B) taken from Ref. [25].*

At equilibrium, the skyrmions arrange in a honeycomb structure (see Fig. 2B), which is reflected in the SANS measurements by the presence of 6 diffraction spots in reciprocal space (see Fig. 10A). The spots disappear in the conical phase [22, 24].

In LTEM experiments, a high-energy beam of electrons is incident on a thin (100nm) specimen of a magnet displaying non-uniform magnetization. The magnetic texture gives rise to a local variation of the magnetization within the specimen, which in turn creates variations in the local magnetic field. Electrons passing through different regions of magnetization will experience distinct Lorentz forces which result in the formation of interference

[24]There are current efforts directed at employing resonant soft X-ray scattering for detecting skyrmions. This technique, however, is still to be demonstrated [119].

pattern at defocused positions [121]. With help of transport-of-intensity equations [122], the in-plane magnetization of the sample can be recovered from the measurements [22, 121]. Although the technique is limited to only in-plane magnetization imaging, it is powerful enough to allow the resolution of magnetic structures at nanometer scales and has been successfully employed to visualize single skyrmions[25] (see Fig. 10B).

Both of these techniques involve sophisticated experimental set-ups. It is clear that for a successfully incorporation of skyrmionics into commercial devices the complexity of the detection methods must be reduced. A promising direction strives to use all-electrical means, which has the advantage of being compatible with current electronic technology [123]. In 2015, the fist electrical detection of skyrmions was carried out by Hanneken *et al.* [26] and followed by Crum *et al.* [124]. Their experiments exploited the difference in tunneling magnetoresistance arising from the non-collinear texture of skyrmions compared with the uniformly magnetized background. Today, a great variety of magneto-transport phenomena have been proposed [123], some of them include: the anomalous Hall effect [125], the topological Hall effect [22], and the SMR [28]. The latter being the topic of the following section.

4 All-electric detection of magnetic textures

With the necessary theoretical background to comprehend the main theory for SMR, and with a better understanding of various magnetic textures displayed by crystals, we proceed with the description of the method by which SMR can distinguish these textures.

4.1 SMR-detection

In section 2.2, we discussed how the transverse and longitudinal resistance of a NM in contact with an insulating FM depend on the magnetization direction of the FM. The dependence is given in Eqs. 19. Eqs. 19 was derived under the assumption that the magnetization of the insulating FM was uniform. Clearly, this condition no longer holds for more complicated magnetic orders such as helices, cones, and skyrmions. However, if the length scale at which the magnetic texture changes are much bigger than the spin diffusion length[25], the SMR can be locally calculated using Eqs. 19 (see Fig. 11A). Thus, the resulting resistance would be the sum of each individual surface contribution [28]. Mathematically, this is equivalent to replacing the products of the magnetization in 19 by their average values. This is expressed in Eqs. 26 where the average (<>) is taken over the NM|FM interface.

$$\begin{aligned}\rho_{\text{long}} &= \rho + \Delta\rho_0 + \Delta\rho_1\langle m_x^2 + m_z^2\rangle \\ \rho_{\text{trans}} &= \Delta\rho_1\langle m_x m_y\rangle + \Delta\rho_2\langle m_z\rangle\end{aligned} \tag{26}$$

In general, different magnetic textures have different magnetization averages for the same applied magnetic field. Therefore, it is possible to use the measurements of the SMR as a function of applied magnetic field to determine the presence of a particular spin order. Take for example the case of a collinear magnetic arrangement in an in-plane external magnetic field. In this situation, the magnetization direction coincides with the direction of the applied magnetic field[26]. If we denote by α the angle between the applied field and the longitudinal current (see Fig. 7), then $(m_x, m_y, m_z) = (\cos(\alpha), \sin(\alpha), 0)$. Substituting those values in equation 26 implies that the transverse resistance should shown a $m_x m_y = \cos(\alpha)\sin(\alpha) = 2\sin(2\alpha)$ dependence. This is illustrated in figure 11C.

If instead, a conical magnetic order is present in the FM, the magnetization direction will be given by Eq. 27, where θ is the cone angle, $\vec{Q}$ is the spiral pitch direction, and $\{\hat{e}_i\}$ form a right-handed orthogonal basis. When an external magnetic field is applied, $\hat{e}_3$ and $\vec{Q}$ are parallel to the field direction.

$$\vec{m} = \cos(\theta)\hat{e}_3 + \sin(\theta)(\hat{e}_1\cos(\vec{Q}\cdot\vec{x}) + \hat{e}_2\sin(\vec{Q}\cdot\vec{x})) \tag{27}$$

Substituting Eq. 27 in Eq. 26 gives Eq. 28 [28]. In addition to the $\sin(2\alpha)$ dependence, which is the same as for the uniform magnetic state, ρ_{trans} depends on the cone angle θ that decreases with increasing magnetic field. Eq. 28 implies that the amplitude of the SMR resistance decreases until $\cos(\theta) = 1/\sqrt{3}$. Subsequently, the amplitude changes signs, or equivalently, the SMR phase changes by π. This is illustrated in Fig. 11C.

$$\rho_{\text{trans}} \propto \sin(2\alpha)(3\cos^2(\theta) - 1) \tag{28}$$

[25] For example, in spirals arraignments, this length scale would be related to the spiral period.

[26] Assuming the system is isotropic in the xy directions and that the magnetic field is strong enough to complete saturate the FM.

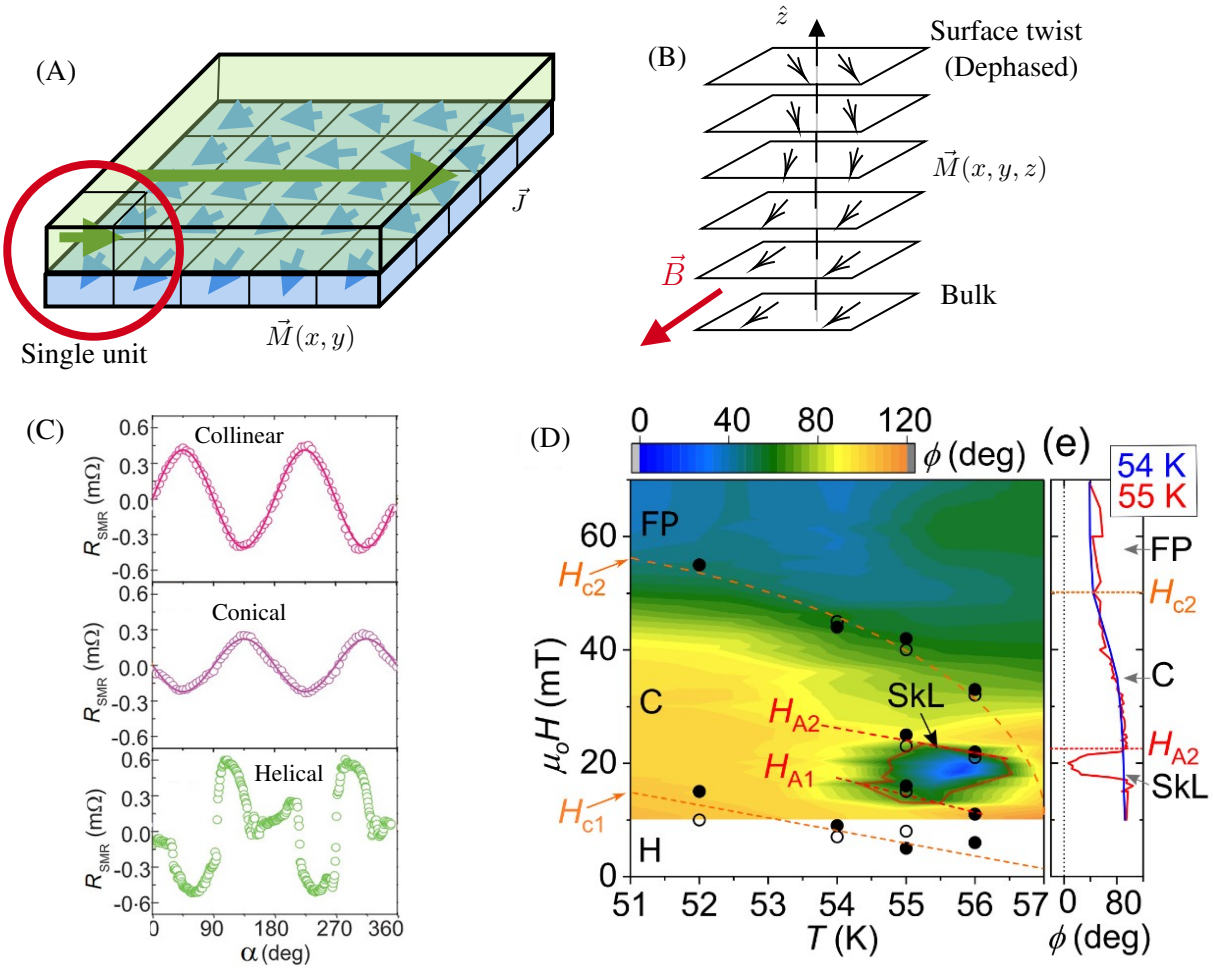

Figure 11: *(A) When the spin diffusion length is smaller than the variations at which magnetization changes, we divide the bilayer structures into units. Each unit will effectively experience a uniform magnetization and thus, the total SMR signal will be the sum of each unit contribution, i.e. the SMR signal will be averaged over the surface. (B) Due to bulk DMI, a surface twist is present; therefore, the SMR signal will be given by a magnetization different from the bulk magnetization. (C) Expected signal of the SMR as a function of applied magnetic field angle. Graphs adapted from [28]. The conical signal represents the change of sign of the SMR signal. (D) Measured phase of the SMR in a Pt|CSO structure. The black and white dots represents the bulk-phase boundaries of the CSO crystal. The contour plot closely resembles the magnetic phase diagram (see Fig. 12). Image taken from [42].*

A similar analysis can be carried out for other spin textures such as helices and skyrmions [28, 42], their analysis is complicated and lies outside the scopes of the present work. One of the SMR signals for the helical phase is illustrated in Fig. 11C. In general, the angle dependence (α) turns out to be different enough to distinguish between the various magnetic phases.

In summary, to electrically detect a magnetic textures, the SMR signal is measured as a function of the angle α. By determining the corresponding amplitude and phase information of this signal, as well as deviations from the $\sin(2\alpha + \phi)$ behavior, the signal can be related to a unique magnetization texture.

4.2 Experimental studies

The experimental procedure described in the previous sections have been carried out by Aqeel *et al.* in 2016 [28]. In their experiments, the transverse resistance as a function of an applied magnetic field was measured in a Pt|CSO bilayer structure. The experiment was carried out at a temperature of 5 K and the different magnetic phases were explored by changing the **magnitude** of the applied magnetic field. At that temperature, CSO displays 5 distinct magnetic arrangements: helical, conical, tilted spiral, low-temperature skyrmion state, and field polarized [FP] or collinear state (see Fig. 12)[113]. Their results, however, could only determine the presence of the helical, conical, and collinear textures. In this

regard, the expected decrease of SMR amplitude in the conical region was observed, in agreement with Eq. 28. The absence of a tilted conical and low-temperature skyrmion phase in the SMR detection could be due to the fact that not enough values of the SMR amplitude with magnetic field magnitude were measured.

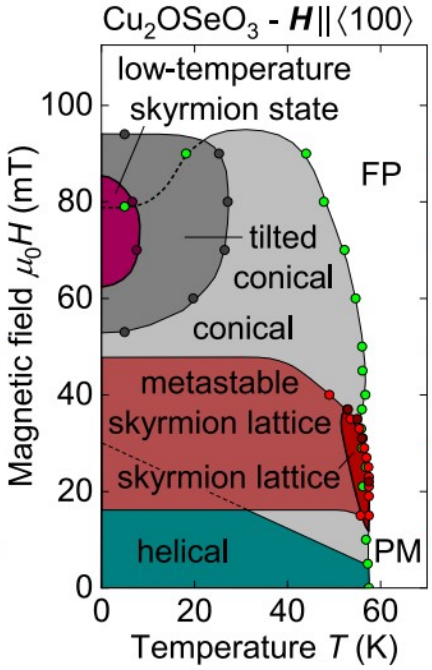

Figure 12: *Magnetic phase diagram of CSO. FP = Field polarized. PM = paramagnetic. Image taken from [113].*

In 2021, Aqeel *et al.* performed the same type of experiments at higher temperature to explore the skyrmionic lattice of CSO. Their findings showed a considerable disagreement to those predicted by Eq. 26. To begin, the dependence of the SMR signal on the strength of the magnetic field was not reproduced. The SMR resistance in the conical spiral state decreased as the magnetic field increased for all fields $B < B_{c2}$, while Eq. 28 predicts that the SMR amplitude should decrease for $\theta \lessapprox 55.7$ and then increase as the spins in the conical spiral become more and more aligned with the applied field. Moreover, they also reported a constant phase shift of the $\sin(2\alpha)$ in the SMR signal. This effect is observed even in the collinear case. A phase shift implies that the magnetization experienced by the SMR at the interface is different from the bulk magnetization of the insulating FM. These observations are even more puzzling since it appears to contradict their previous findings at low temperature (T=5K) where no phase shift was detected for the collinear case and the Eq. 28 was reproduced [28].

To account for the discrepancy in the SMR amplitude as a function of the magnitude of the applied field, new phenomenological terms were added to the expression for ρ_{trans} on the basis of symmetry arguments. This procedure bares close resemblece to the discussion of the OHE in section 2.1. Eq. 26 was replaced by Eq. 29, where A, B, and C are treated as phenomenological constants. The best fit of experimental data was obtained for $C = 0$ and $B = -1.59A/|Q|$. To this day, the microscopic origin of this phenomenological parameters is not well understood. A corollary of Eq. 29 is the fact that the phenomenological expression given in Eq. 19 are uniquely determined by the symmetry of the device.

$$\rho_{\text{trans}} = A\langle m_x m_y\rangle + B\langle m_z \tfrac{\partial m_x}{\partial y} - \tfrac{\partial m_z}{\partial y} m_x\rangle + C\langle m_z^2 m_x m_y\rangle, \quad (29)$$

To explain the constant phase shift, Aqeel *et al.* appeal to the Dilashenskii-Morija interaction in the free energy density expansion given by Eq. 22. The presence of an interface breaks the symmetry requirements for the solutions. As a consequence, the state of minimum energy is no longer a uniform collinear phase, but rather, an arrangements with a twist near the surface (see Fig. 11B). With this in mind, the magnetization direction at the surface would always be shifted compared with the bulk magnetization, thus accounting for the constant phase shift.

The breaking of symmetry at the interface has additional consequences for the other spin textures. For example, the conical phase would also experience a constant shift combined with a contraction of the cone angle. This contraction effectively diminish the necessary magnitude of the magnetic field required to achieve the collinear state at the interface, and thus should be reflected in the SMR since it is only sensitive to surface magnetization. This effect, was not observed (see Fig. 11D), which motivated Aqeel *et al.* to introduce interfacial DMI and surface anisotropy [42].

In summary, three main corrections to the current theory were necessary: (1) a constant surface twist originating from **bulk** DMI, (2) the addition of new phenomenological terms in the expression for the magnetoresistance, and (3) the introduction of interfacial DMI and surface anisotropy. Nevertheless, by just looking at the measurements of SMR phase and amplitude —disregarding their origin— it is possible to recover the presence of the

skyrmion lattice [SkL]. This phase is characterized by significant diminish in the SMR phase as compared with the values for the conical phase as can be seen in Fig. 11D.

4.3 Discussion

The current theoretical description of SMR correctly captures the experimental behavior reported in collinear insulating ferrimagnets as was discussed in section 2.2 [30]. The practical results for collinear states are robust enough that the implementation of SMR measurements in commercial devices seems possible in the near future, the main challenges being the control of the growth and mass-production of insulating FM.

On the other hand, the theoretical assumptions underlying Chen's *et al.* theory [34] continue to be opened to debate. Indeed, as was commented in section 4.2, the physical elements of this theory should be equally valid for non-uniform magnetic states, yet significant experimental mismatch is observed. The possibility of systematic errors in the experiments discussed in section 4.2 cannot be ruled out[27]. However, we believe that the discrepancies are significant enough that questions can be raised about the validity of some of the theoretical assumptions underlying this theory.

In our opinion, two points stand out. Firstly, the theoretical model was deduced under the assumption of no-external magnetic field. This situation is far from what is present in the experiments in which an external magnetic field is required to sustain the magnetic texture. The inclusion of this field would have impacts in the diffusion equations such as Eq. 14. Indeed, Dyakonov and Perel already commented in their seminal paper [59] on the SHE that an external magnetic field could destroy the spin current. The presence of this external field in the theoretical model could also have consequences for coherent effects; for example, a coherent procession of the electron spin could occur near the boundary, giving rise to a more complicated magnetoresistance than the one described in section 2.2.

The second point concerns the boundary conditions stated in Eq. 10. The assumption of a perfect insulator may not hold for CSO which would require the introduction of parallel currents. The deviations from a perfect insulator could lead to some of the carriers exploring "more of the bulk" explaining why the magnetic phase transitions measured with SMR still occurred at their bulk values ignoring the cone contraction.

Finally, we should not be surprised by the fact that Chen's *et al.* model correctly predicts the magnetic field dependence in Eq. 19. The deduction of the symmetry allowed phenomenological terms in Eq. 26 shows that those expressions are the only combinations allowed by symmetry. Indeed, the fact that Vlietstra *et al.* [92] could not recover the functional dependence of the coefficients predicted by Chen's *et al.* (see section 2.2) should be interpreted as another point of concern. That is the power of symmetry arguments, it does not matter which microscopic theory or assumptions one uses, as long as they are consistent with the symmetry of the system, the same phenomenological relationship will be obtained. Therefore, a more robust test of a theory for SMR must come from the correct determination of the values of $\Delta\rho$. This will not be without its challenges, as previously mentioned, interfacial disorder and the quality of deposition plays a significant role in the values of parameters of the model such as spin-mixing conductance and Hall angle.

Perhaps, advances in deposition techniques such as pulsed laser deposition [PLD] may be able to create devices with expitaxially smooth surfaces which could be use to further test the current theory for SMR.

5 Final Remarks

Leaving aside the theoretical aspects of SMR. The method presents a series of advantages and disadvantages: (1) it substitutes SANS and LTEM by simple —but tricky— magnetotransport experiments. Both SANS and LTEM have straightforward interpretation but complicated set-ups, while SMR has the ease in experimentation but complicated interpretations. (2) SMR does not require current to pass through the FM layer, thus it could prevent heating and degradation due to currents. Indeed, even in the simple collinear case, the technique has te potential to reduce power consumption due to cooling [34]. (3) SMR is a surface sensitive technique, but it does not explore the full topological properties of skyrmions and thus is not the ultimate candidate for skyrmionic devices. Nevertheless, we believe that a secondary role is still possible.

Adding to this last point, the authors of this work, do

[27] Here, it is worth remembering that the detection of the SHE and ISHE also started with a significant experimental mismatch [60, 61]

not believe that —in its current state— SMR can be successfully incorporated in skyrmionic applications. Too many open questions still remain. This, however, can have positive consequences, as research in SMR may shed light in fundamental aspects for spintronics.

6 Acknowledgments

We would like to express our must sincere gratitude to prof. Maxim Mostovoy for his supervision during the project. We would also like to thank prof. Maxim Pchenitchnikov, prof. Tamalika Banerjee, prof. Patrick Onck, and Donato Ottomano for the preparation of tutorials and workshops. One final thanks to Tsedenia Zewdie for her comments and feedback on the first draft of this work and to Krishna Raajan Sundararajan for sharing useful references.

6 References

1. Feynman, R. P. There's plenty of room at the bottom. *Engineering and science* **23** (1959).
2. Information Storage Industry Consorsium. *INSIC's 2019-2029 Application, Systems and Technology Roadmap* Accessed: 2022-03-10. 2019. https://insic.org/insic-application-systems-and-technology-roadmap/.
3. Goda, K. & Kitsuregawa, M. The history of storage systems. *Proceedings of the IEEE* **100,** 1433–1440 (2012).
4. International Business Machines Corporation. *650 RAMAC fact sheet* Accessed: 2022-03-10. 1959. https://www.ibm.com/ibm/history/exhibits/650/650_tr2.html.
5. International Business Machines Corporation. *IBM 355 disk storage unit* Accessed: 2022-03-10. 1956. https://www.ibm.com/ibm/history/exhibits/storage/storage_355.html.
6. Computer History Museum. *Timeline of Computer History* Accessed: 2022-03-10. https://www.computerhistory.org/timeline/memory-storage/.
7. Fontana, R. E., Hetzler, S. & Decad, G. M. *IBM Areal Density Comparison Paper 1 Tape Based Magnetic Recording : Technology Landscape Comparisons with Hard Disk Drive and Flash Roadmaps* **in** (2011).
8. The Brainy Insight. *Cloud Storage Market Size by Component (Solution, Services), Deployment Type (Private, Public, Hybrid), User Type, Industry Vertical, Regions, Global Industry Analysis, Share, Growth, Trends, and Forecast 2021 to 2028* Accessed: 2022-03-10. 2021. https://www.thebrainyinsights.com/report/cloud-storage-market-12592.
9. Grochowski, E. & Hoyt, R. F. Future trends in hard disk drives. *IEEE transactions on Magnetics* **32,** 1850–1854 (1996).
10. Hanson, G. W. *Fundamentals of nanoelectronics. Chapter 1.* (Prentice Hall, 2008).
11. Jin, Y., Shihab, M. & Jung, M. *Area, power, and latency considerations of STT-MRAM to substitute for main memory* **in** *Proc. ISCA* (2014).
12. Weller, D. & Moser, A. Thermal effect limits in ultrahigh-density magnetic recording. *IEEE Transactions on Magnetics* **35,** 4423–4439 (1999).
13. Kryder, M. *Magnetic recording beyond the superparamagnetic limit* **in** *2000 IEEE International Magnetics Conference (INTERMAG)* (2000), 575–575.
14. Wood, R. The feasibility of magnetic recording at 1 Terabit per square inch. *IEEE Transactions on Magnetics* **36,** 36–42 (2000).
15. Wolf, S. A., Chtchelkanova, A. Y. & Treger, D. M. Spintronics—A retrospective and perspective. *IBM Journal of Research and Development* **50,** 101–110 (2006).
16. Hirohata, A., Yamada, K., Nakatani, Y., Prejbeanu, I.-L., Diény, B., Pirro, P. & Hillebrands, B. Review on spintronics: Principles and device applications. *Journal of Magnetism and Magnetic Materials* **509,** 166711 (2020).
17. Fert, A. The present and the future of spintronics. *Thin Solid Films* **517,** 2–5 (2008).
18. Barla, P., Joshi, V. K. & Bhat, S. Spintronic devices: a promising alternative to CMOS devices. *Journal of Computational Electronics* **20,** 805–837 (2021).
19. Fert, A., Cros, V. & Sampaio, J. Skyrmions on the track. *Nature nanotechnology* **8,** 152–156 (2013).

20. Göbel, B., Mertig, I. & Tretiakov, O. A. Beyond skyrmions: Review and perspectives of alternative magnetic quasiparticles. *Physics Reports* **895,** 1–28 (2021).

21. Je, S.-G., Han, H.-S., Kim, S. K., Montoya, S. A., Chao, W., Hong, I.-S., Fullerton, E. E., Lee, K.-S., Lee, K.-J., Im, M.-Y. **andothers**. Direct demonstration of topological stability of magnetic skyrmions via topology manipulation. *ACS nano* **14,** 3251–3258 (2020).

22. Nagaosa, N. & Tokura, Y. Topological properties and dynamics of magnetic skyrmions. *Nature nanotechnology* **8,** 899–911 (2013).

23. Back, C., Cros, V., Ebert, H., Everschor-Sitte, K., Fert, A., Garst, M., Ma, T., Mankovsky, S., Monchesky, T., Mostovoy, M. **andothers**. The 2020 skyrmionics roadmap. *Journal of Physics D: Applied Physics* **53,** 363001 (2020).

24. Mühlbauer, S., Binz, B., Jonietz, F., Pfleiderer, C., Rosch, A., Neubauer, A., Georgii, R. & Böni, P. Skyrmion lattice in a chiral magnet. *Science* **323,** 915–919 (2009).

25. Yu, X., Onose, Y., Kanazawa, N., Park, J. H., Han, J., Matsui, Y., Nagaosa, N. & Tokura, Y. Real-space observation of a two-dimensional skyrmion crystal. *Nature* **465,** 901–904 (2010).

26. Hanneken, C., Otte, F., Kubetzka, A., Dupé, B., Romming, N., Von Bergmann, K., Wiesendanger, R. & Heinze, S. Electrical detection of magnetic skyrmions by tunnelling non-collinear magnetoresistance. *Nature nanotechnology* **10,** 1039–1042 (2015).

27. Romming, N., Hanneken, C., Menzel, M., Bickel, J. E., Wolter, B., von Bergmann, K., Kubetzka, A. & Wiesendanger, R. Writing and deleting single magnetic skyrmions. *Science* **341,** 636–639 (2013).

28. Aqeel, A., Vlietstra, N., Roy, A., Mostovoy, M., Van Wees, B. & Palstra, T. Electrical detection of spiral spin structures in Pt— Cu 2 OSeO 3 heterostructures. *Physical Review B* **94,** 134418 (2016).

29. Weiler, M., Althammer, M., Czeschka, F. D., Huebl, H., Wagner, M. S., Opel, M., Imort, I.-M., Reiss, G., Thomas, A., Gross, R. **andothers**. Local charge and spin currents in magnetothermal landscapes. *Physical review letters* **108,** 106602 (2012).

30. Chen, Y.-T., Takahashi, S., Nakayama, H., Althammer, M., Goennenwein, S. T., Saitoh, E. & Bauer, G. E. Theory of spin Hall magnetoresistance (SMR) and related phenomena. *Journal of Physics: Condensed Matter* **28,** 103004 (2016).

31. Huang, S. Y., Fan, X., Qu, D., Chen, Y. P., Wang, W. G., Wu, J., Chen, T. Y., Xiao, J. Q. & Chien, C. L. Transport Magnetic Proximity Effects in Platinum. *Phys. Rev. Lett.* **109,** 107204 (2012).

32. Nickel, J. *Magnetoresistance overview* (Hewlett-Packard Laboratories, Technical Publications Department Palo Alto . . ., 1995).

33. Wilhelm, F., Poulopoulos, P., Ceballos, G., Wende, H., Baberschke, K., Srivastava, P., Benea, D., Ebert, H., Angelakeris, M., Flevaris, N. **andothers**. Layer-resolved magnetic moments in Ni/Pt multilayers. *Physical review letters* **85,** 413 (2000).

34. Chen, Y.-T., Takahashi, S., Nakayama, H., Althammer, M., Goennenwein, S. T., Saitoh, E. & Bauer, G. E. Theory of spin Hall magnetoresistance. *Physical Review B* **87,** 144411 (2013).

35. Nakayama, H., Althammer, M., Chen, Y.-T., Uchida, K.-i., Kajiwara, Y., Kikuchi, D., Ohtani, T., Geprägs, S., Opel, M., Takahashi, S. **andothers**. Spin Hall magnetoresistance induced by a nonequilibrium proximity effect. *Physical review letters* **110,** 206601 (2013).

36. Ahmed, A. S., Lee, A. J., Bagués, N., McCullian, B. A., Thabt, A. M., Perrine, A., Wu, P.-K., Rowland, J. R., Randeria, M., Hammel, P. C. **andothers**. Spin-Hall topological Hall effect in highly tunable Pt/ferrimagnetic-insulator bilayers. *Nano letters* **19,** 5683–5688 (2019).

37. Daniels, M. W., Yu, W., Cheng, R., Xiao, J., Xiao, D. **andothers**. Topological spin Hall effects and tunable skyrmion Hall effects in uniaxial antiferromagnetic insulators. *Physical Review B* **99,** 224433 (2019).

38. Ding, S., Ross, A., Lebrun, R., Becker, S., Lee, K., Boventer, I., Das, S., Kurokawa, Y., Gupta, S., Yang, J. **andothers**. Interfacial Dzyaloshinskii-Moriya interaction and chiral magnetic textures in a ferrimagnetic insulator. *Physical Review B* **100,** 100406 (2019).

39. Cheng, Y., Yu, S., Zhu, M., Hwang, J. & Yang, F. Evidence of the topological Hall effect in Pt/Antiferromagnetic insulator bilayers. *Physical Review Letters* **123,** 237206 (2019).

40. Shao, Q., Liu, Y., Yu, G., Kim, S. K., Che, X., Tang, C., He, Q. L., Tserkovnyak, Y., Shi, J. & Wang, K. L. Topological Hall effect at above room temperature in heterostructures composed of a magnetic insulator and a heavy metal. *Nature Electronics* **2,** 182–186 (2019).

41. Althammer, M. All-Electrical Magnon Transport Experiments in Magnetically Ordered Insulators. *physica status solidi (RRL)–Rapid Research Letters* **15,** 2100130 (2021).

42. Aqeel, A., Azhar, M., Vlietstra, N., Pozzi, A., Sahliger, J., Huebl, H., Palstra, T., Back, C. & Mostovoy, M. All-electrical detection of skyrmion lattice state and chiral surface twists. *Physical Review B* **103,** L100410 (2021).

43. Hall, E. H. **andothers**. On a new action of the magnet on electric currents. *American Journal of Mathematics* **2,** 287–292 (1879).

44. Ladstone, G. The discovery of the Hall effect. *Physics Education* **14** (1979).

45. Kittel, C. & McEuen, P. *Kittel's Introduction to Solid State Physics. Chapter 6. Free Electron Fermi Gas* (John Wiley & Sons, 2018).

46. Bulman, W. Applications of the Hall effect. *Solid-State Electronics* **9,** 361–372 (1966).

47. Karsenty, A. A comprehensive review of integrated Hall effects in macro-, micro-, nanoscales, and quantum devices. *Sensors* **20,** 4163 (2020).

48. Ashcroft, N. W. & Mermin, N. D. *Solid State Physics* (Holt-Saunders, 1976).

49. Simon, S. H. *The Oxford solid state basics. Chapter 3. Electrons in Fields* (OUP Oxford, 2013).

50. National Institute for Standards and Technology. *Hall Effect Measurements* Accessed: 2022-03-21. 2005. https://web.archive.org/web/20080321004447/http://www.eeel.nist.gov/812/hall.html.

51. Kasap, S. Hall effect in semiconductors. *Electron. Booklet* **1** (2001).

52. Yu, L., Cheung, K., Tilak, V., Dunne, G., Matocha, K., Campbell, J., Suehle, J. & Sheng, K. *A fast, simple wafer-level Hall-mobility measurement technique* **in** *2009 IEEE International Integrated Reliability Workshop Final Report* (2009), 73–76.

53. Richard P. Feynman. *Symmetry in Physical Laws* Accessed: 2022-04-14. https://www.feynmanlectures.caltech.edu/I_52.html.

54. Sinova, J., Valenzuela, S. O., Wunderlich, J., Back, C. & Jungwirth, T. Spin hall effects. *Reviews of Modern Physics* **87,** 1213 (2015).

55. Dirac, P. A. M. The quantum theory of the electron. *Proceedings of the Royal Society of London. Series A, Containing Papers of a Mathematical and Physical Character* **117,** 610–624 (1928).

56. Tolhoek, H. Electron polarization, theory and experiment. *Reviews of modern physics* **28,** 277 (1956).

57. Mott, N. F. The scattering of fast electrons by atomic nuclei. *Proceedings of the Royal Society of London. Series A, Containing Papers of a Mathematical and Physical Character* **124,** 425–442 (1929).

58. Shull, C. G., Chase, C. & Myers, F. Electron polarization. *Physical Review* **63,** 29 (1943).

59. Dyakonov, M. I. & Perel, V. Current-induced spin orientation of electrons in semiconductors. *Physics Letters A* **35,** 459–460 (1971).

60. Mihajlović, G., Pearson, J., Garcia, M., Bader, S. & Hoffmann, A. Negative nonlocal resistance in mesoscopic gold Hall bars: absence of the giant spin Hall effect. *Physical review letters* **103,** 166601 (2009).

61. Brüne, C., Roth, A., Novik, E., König, M., Buhmann, H., Hankiewicz, E., Hanke, W., Sinova, J. & Molenkamp, L. Evidence for the ballistic intrinsic spin Hall effect in HgTe nanostructures. *Nature Physics* **6,** 448–454 (2010).

62. Hirsch, J. Spin hall effect. *Physical review letters* **83,** 1834 (1999).

63. Zhang, S. Spin Hall effect in the presence of spin diffusion. *Physical review letters* **85,** 393 (2000).

64. Bergmann, G. The anomalous Hall effect. *physics today* **32,** 25–30 (1979).

65. Idzuchi, H., Fukuma, Y. & Otani, Y. Towards coherent spin precession in pure-spin current. *Scientific reports* **2,** 1–5 (2012).

66. Dyakonov, M. I. & Khaetskii, A. *Spin physics in semiconductors.Spin Hall Effect.* (Springer, 2008).

67. Kondepudi, D. & Prigogine, I. *Modern thermodynamics: from heat engines to dissipative structures* (John Wiley & Sons, 2014).

68. Callen, H. B. *Thermodynamics and an Introduction to Thermostatistics* 1998.

69. Onsager, L. Reciprocal relations in irreversible processes. I. *Physical review* **37,** 405 (1931).

70. Onsager, L. Reciprocal relations in irreversible processes. II. *Physical review* **38,** 2265 (1931).

71. Bauer, G. E., Saitoh, E. & Van Wees, B. J. Spin caloritronics. *Nature materials* **11,** 391–399 (2012).

72. Keller, S., Mihalceanu, L., Schweizer, M. R., Lang, P., Heinz, B., Geilen, M., Brächer, T., Pirro, P., Meyer, T., Conca, A. **andothers**. Determination of the spin Hall angle in single-crystalline Pt films from spin pumping experiments. *New Journal of Physics* **20,** 053002 (2018).

73. Wang, H., Du, C., Pu, Y., Adur, R., Hammel, P. C. & Yang, F. Scaling of spin Hall angle in 3d, 4d, and 5d metals from Y 3 Fe 5 O 12/metal spin pumping. *Physical review letters* **112,** 197201 (2014).

74. Atkins, P. W. & Friedman, R. S. *Molecular quantum mechanics. Chapter 7. Atomic spectra and atomic structure* (Oxford university press, 2011).

75. Burrowes, C. & Heinrich, B. **in** *Magnonics: From Fundamentals to Applications. Spin Pumping at Ytrium Iron Garnet Interfaces* (**editors** Demokritov, S. O. & Slavin, A. N.) 129–141 (Springer Berlin Heidelberg, Berlin, Heidelberg, 2013). ISBN: 978-3-642-30247-3.

76. Takahashi, S. **in** *Handbook of Spintronics. Physical Principles of Spin Pumping* (**editors** Xu, Y., Awschalom, D. D. & Nitta, J.) 1445–1480 (Springer Netherlands, Dordrecht, 2016). ISBN: 978-94-007-6892-5.

77. Brataas, A., Nazarov, Y. V. & Bauer, G. E. Finite-element theory of transport in ferromagnet–normal metal systems. *Physical Review Letters* **84,** 2481 (2000).

78. Brataas, A., Bauer, G. E. & Kelly, P. J. Non-collinear magnetoelectronics. *Physics Reports* **427,** 157–255 (2006).

79. Maekawa, S. *Concepts in spin electronics* (OUP Oxford, 2006).

80. Maciel, N., Marques, E., Naviner, L., Zhou, Y. & Cai, H. Magnetic tunnel junction applications. *Sensors* **20,** 121 (2019).

81. The Nobel Prize. *The Nobel Prize in Physics 2007* Accessed: 2022-03-10. 2007. https://www.nobelprize.org/prizes/physics/2007/summary/.

82. Slonczewski, J. C. Current-driven excitation of magnetic multilayers. *Journal of Magnetism and Magnetic Materials* **159,** L1–L7 (1996).

83. Zhang, Q., Hikino, S.-i. & Yunoki, S. First-principles study of the spin-mixing conductance in Pt/Ni81Fe19 junctions. *Applied Physics Letters* **99,** 172105 (2011).

84. Schep, K. M., Kelly, P. J. & Bauer, G. E. Giant magnetoresistance without defect scattering. *Physical review letters* **74,** 586 (1995).

85. Bauer, G. E., Schep, K. M., Xia, K. & Kelly, P. J. Scattering theory of interface resistance in magnetic multilayers. *Journal of physics D: applied physics* **35,** 2410 (2002).

86. Schep, K. M., van Hoof, J. B., Kelly, P. J., Bauer, G. E. & Inglesfield, J. E. Interface resistances of magnetic multilayers. *Physical Review B* **56,** 10805 (1997).

87. Freimuth, F., Blügel, S. & Mokrousov, Y. Anisotropic spin Hall effect from first principles. *Physical review letters* **105,** 246602 (2010).

88. Johnson, M. Analysis of anomalous multilayer magnetoresistance within the thermomagnetoelectric system. *Physical review letters* **67,** 3594 (1991).

89. Johnson, M. & Silsbee, R. Thermodynamic analysis of interfacial transport and of the thermomagnetoelectric system. *Physical Review B* **35,** 4959 (1987).

90. Van Son, P., Van Kempen, H. & Wyder, P. Boundary resistance of the ferromagnetic-nonferromagnetic metal interface. *Physical Review Letters* **58,** 2271 (1987).

91. Valet, T. & Fert, A. Theory of the perpendicular magnetoresistance in magnetic multilayers. *Physical Review B* **48,** 7099 (1993).

92. Vlietstra, N., Shan, J., Castel, V., Van Wees, B. & Youssef, J. B. Spin-Hall magnetoresistance in platinum on yttrium iron garnet: Dependence on platinum thickness and in-plane/out-of-plane magnetization. *Physical Review B* **87,** 184421 (2013).

93. Vlietstra, N., Shan, J., Castel, V., Ben Youssef, J., Bauer, G. & Van Wees, B. Exchange magnetic field torques in YIG/Pt bilayers observed by the spin-Hall magnetoresistance. *Applied Physics Letters* **103,** 032401 (2013).

94. Ding, Z., Chen, B., Liang, J., Zhu, J., Li, J. & Wu, Y. Spin Hall magnetoresistance in Pt/Fe 3 O 4 thin films at room temperature. *Physical Review B* **90,** 134424 (2014).

95. Isasa, M., Bedoya-Pinto, A., Vélez, S., Golmar, F., Sánchez, F., Hueso, L. E., Fontcuberta, J. & Casanova, F. Spin Hall magnetoresistance at Pt/CoFe2O4 interfaces and texture effects. *Applied Physics Letters* **105,** 142402 (2014).

96. Qu, D., Huang, S., Hu, J., Wu, R. & Chien, C. Intrinsic spin Seebeck effect in Au/YIG. *Physical review letters* **110,** 067206 (2013).

97. Saitoh E, Nakayama H and Harii K. *Magnetic sensor and magnetic-storage device Japanese Patent Specification WO 2010110297 A1* Accessed: 2022-04-14. 2010. https://www.j-platpat.inpit.go.jp/p0200.

98. Kaplan, T. & Mahanti, S. On the Bohr-van Leeuwen theorem, the non-existence of classical magnetism in thermal equilibrium. *EPL (Europhysics Letters)* **87,** 17002 (2009).

99. Landau, L. D. & Lifshitz, E. M. *Statistical Physics: Volume 5 Vol. 5* 2013.

100. Lancaster, T. & Blundell, S. J. *Quantum field theory for the gifted amateur* (OUP Oxford, 2014).

101. Kardar, M. *Statistical physics of fields* (Cambridge University Press, 2007).

102. Dzyaloshinsky, I. A thermodynamic theory of "weak" ferromagnetism of antiferromagnetics. *Journal of physics and chemistry of solids* **4,** 241–255 (1958).

103. Blundell, S. *Magnetism in condensed matter* 2003.

104. Moriya, T. Anisotropic superexchange interaction and weak ferromagnetism. *Physical review* **120,** 91 (1960).

105. Bak, P. & Jensen, M. H. Theory of helical magnetic structures and phase transitions in MnSi and FeGe. *Journal of Physics C: Solid State Physics* **13,** L881 (1980).

106. Bogdanov, A. & Yablonskii, D. Thermodynamically stable "vortices" in magnetically ordered crystals. The mixed state of magnets. *Zh. Eksp. Teor. Fiz* **95,** 182 (1989).

107. Skyrme, T. H. R. A unified field theory of mesons and baryons. *Nuclear Physics* **31,** 556–569 (1962).

108. Yu, X., Kanazawa, N., Zhang, W., Nagai, T., Hara, T., Kimoto, K., Matsui, Y., Onose, Y. & Tokura, Y. Skyrmion flow near room temperature in an ultralow current density. *Nature communications* **3,** 1–6 (2012).

109. Okubo, T., Chung, S. & Kawamura, H. Multiple-q states and the skyrmion lattice of the triangular-lattice Heisenberg antiferromagnet under magnetic fields. *Physical review letters* **108,** 017206 (2012).

110. Heinze, S., Von Bergmann, K., Menzel, M., Brede, J., Kubetzka, A., Wiesendanger, R., Bihlmayer, G. & Blügel, S. Spontaneous atomic-scale magnetic skyrmion lattice in two dimensions. *nature physics* **7,** 713–718 (2011).

111. Bauer, A. & Pfleiderer, C. **in** *Topological Structures in Ferroic Materials* 1–28 (Springer, 2016).

112. Karube, K., White, J., Reynolds, N., Gavilano, J., Oike, H., Kikkawa, A., Kagawa, F., Tokunaga, Y., Rønnow, H. M., Tokura, Y. **andothers**. Robust metastable skyrmions and their triangular–square lattice structural transition in a high-temperature chiral magnet. *Nature materials* **15,** 1237–1242 (2016).

113. Chacon, A., Heinen, L., Halder, M., Bauer, A., Simeth, W., Mühlbauer, S., Berger, H., Garst, M., Rosch, A. & Pfleiderer, C. Observation of two independent skyrmion phases in a chiral magnetic material. *Nature Physics* **14,** 936–941 (2018).

114. Cortés-Ortuño, D., Wang, W., Beg, M., Pepper, R. A., Bisotti, M.-A., Carey, R., Vousden, M., Kluyver, T., Hovorka, O. & Fangohr, H. Thermal stability and topological protection of skyrmions in nanotracks. *Scientific reports* **7,** 1–13 (2017).

115. Wang, W., Song, D., Wei, W., Nan, P., Zhang, S., Ge, B., Tian, M., Zang, J. & Du, H. Electrical manipulation of skyrmions in a chiral magnet. *Nature Communications* **13,** 1–7 (2022).

116. Ishikawa, Y., Komatsubara, T. & Bloch, D. Magnetic phase diagram of MnSi. *Physica B+C* **86,** 401–403 (1977).

117. Neubauer, A., Pfleiderer, C., Binz, B., Rosch, A., Ritz, R., Niklowitz, P. & Böni, P. Topological Hall effect in the A phase of MnSi. *Physical review letters* **102,** 186602 (2009).

118. Pappas, C., Lelievre-Berna, E., Falus, P., Bentley, P., Moskvin, E., Grigoriev, S., Fouquet, P. & Farago, B. Chiral paramagnetic skyrmion-like phase in MnSi. *Physical review letters* **102,** 197202 (2009).

119. Van der Laan, G. Soft x-ray resonant magnetic scattering of magnetic nanostructures. *Comptes Rendus Physique* **9,** 570–584 (2008).

120. Dragolici, C. A. *Experimental methods in the study of neutron scattering at small angles* **in** *AIP Conference Proceedings* **1634** (2014), 50–57.

121. Petford-Long, A. & Chapman, J. **in** *Magnetic microscopy of nanostructures* 67–86 (Springer, 2005).

122. Ishizuka, K. & Allman, B. Phase measurement of atomic resolution image using transport of intensity equation. *Journal of electron microscopy* **54,** 191–197 (2005).

123. Fert, A., Reyren, N. & Cros, V. Magnetic skyrmions: advances in physics and potential applications. *Nature Reviews Materials* **2,** 1–15 (2017).

124. Crum, D. M., Bouhassoune, M., Bouaziz, J., Schweflinghaus, B., Blügel, S. & Lounis, S. Perpendicular reading of single confined magnetic skyrmions. *Nature communications* **6,** 1–8 (2015).

125. Nagaosa, N., Sinova, J., Onoda, S., MacDonald, A. H. & Ong, N. P. Anomalous hall effect. *Reviews of modern physics* **82,** 1539 (2010).

SPRINGER NATURE LICENSE
TERMS AND CONDITIONS

May 24, 2022

This Agreement between RUG -- Gustavo Chavez Ponce de Leon ("You") and Springer Nature ("Springer Nature") consists of your license details and the terms and conditions provided by Springer Nature and Copyright Clearance Center.

License Number	5315370876927
License date	May 24, 2022
Licensed Content Publisher	Springer Nature
Licensed Content Publication	Nature Physics
Licensed Content Title	Observation of two independent skyrmion phases in a chiral magnetic material
Licensed Content Author	A. Chacon et al
Licensed Content Date	Jun 25, 2018
Type of Use	Thesis/Dissertation
Requestor type	academic/university or research institute
Format	electronic
Portion	figures/tables/illustrations
Number of figures/tables/illustrations	1

High-res required	no
Will you be translating?	no
Circulation/distribution	1 - 29
Author of this Springer Nature content	no
Title	Student
Institution name	RUG
Expected presentation date	Jun 2022
Order reference number	002
Portions	Figure 1
Requestor Location	RUG Turfsingel 25A Groningen, 9712KH Netherlands Attn: RUG
Total	0.00 USD

Terms and Conditions

Springer Nature Customer Service Centre GmbH
Terms and Conditions

This agreement sets out the terms and conditions of the licence (the **Licence**) between you and **Springer Nature Customer Service Centre GmbH** (the **Licensor**). By clicking 'accept' and completing the transaction for the material (**Licensed Material**), you also confirm your acceptance of these terms and conditions.

1. Grant of License

1. 1. The Licensor grants you a personal, non-exclusive, non-transferable, world-wide licence to reproduce the Licensed Material for the purpose specified in your order only. Licences are granted for the specific use requested in the order and for no other use, subject to the conditions below.

1. 2. The Licensor warrants that it has, to the best of its knowledge, the rights to license reuse of the Licensed Material. However, you should ensure that the material you are requesting is original to the Licensor and does not carry the copyright of another entity (as credited in the published version).

1. 3. If the credit line on any part of the material you have requested indicates that it was reprinted or adapted with permission from another source, then you should also seek permission from that source to reuse the material.

2. Scope of Licence

2. 1. You may only use the Licensed Content in the manner and to the extent permitted by these Ts&Cs and any applicable laws.

2. 2. A separate licence may be required for any additional use of the Licensed Material, e.g. where a licence has been purchased for print only use, separate permission must be obtained for electronic re-use. Similarly, a licence is only valid in the language selected and does not apply for editions in other languages unless additional translation rights have been granted separately in the licence. Any content owned by third parties are expressly excluded from the licence.

2. 3. Similarly, rights for additional components such as custom editions and derivatives require additional permission and may be subject to an additional fee. Please apply to Journalpermissions@springernature.com/bookpermissions@springernature.com for these rights.

2. 4. Where permission has been granted **free of charge** for material in print, permission may also be granted for any electronic version of that work, provided that the material is incidental to your work as a whole and that the electronic version is essentially equivalent to, or substitutes for, the print version.

2. 5. An alternative scope of licence may apply to signatories of the STM Permissions Guidelines, as amended from time to time.

3. Duration of Licence

3. 1. A licence for is valid from the date of purchase ('Licence Date') at the end of the relevant period in the below table:

Scope of Licence	Duration of Licence
Post on a website	12 months
Presentations	12 months
Books and journals	Lifetime of the edition in the language purchased

4. Acknowledgement

4. 1. The Licensor's permission must be acknowledged next to the Licenced Material in print. In electronic form, this acknowledgement must be visible at the same time as the figures/tables/illustrations or abstract, and must be hyperlinked to the journal/book's homepage. Our required acknowledgement format is in the Appendix below.

5. Restrictions on use

5. 1. Use of the Licensed Material may be permitted for incidental promotional use and minor editing privileges e.g. minor adaptations of single figures, changes of format, colour and/or style where the adaptation is credited as set out in Appendix 1 below. Any other changes including but not limited to, cropping, adapting, omitting material that affect the meaning, intention or moral rights of the author are strictly prohibited.

5. 2. You must not use any Licensed Material as part of any design or trademark.

5. 3. Licensed Material may be used in Open Access Publications (OAP) before publication by Springer Nature, but any Licensed Material must be removed from OAP sites prior to final publication.

6. Ownership of Rights

6. 1. Licensed Material remains the property of either Licensor or the relevant third party and any rights not explicitly granted herein are expressly reserved.

7. Warranty

IN NO EVENT SHALL LICENSOR BE LIABLE TO YOU OR ANY OTHER PARTY OR ANY OTHER PERSON OR FOR ANY SPECIAL, CONSEQUENTIAL, INCIDENTAL OR INDIRECT DAMAGES, HOWEVER CAUSED, ARISING OUT OF OR IN CONNECTION WITH THE DOWNLOADING, VIEWING OR USE OF THE MATERIALS REGARDLESS OF THE FORM OF ACTION, WHETHER FOR BREACH OF CONTRACT, BREACH OF WARRANTY, TORT, NEGLIGENCE, INFRINGEMENT OR OTHERWISE (INCLUDING, WITHOUT LIMITATION, DAMAGES BASED ON LOSS OF PROFITS, DATA, FILES, USE, BUSINESS OPPORTUNITY OR CLAIMS OF THIRD PARTIES), AND
WHETHER OR NOT THE PARTY HAS BEEN ADVISED OF THE POSSIBILITY OF SUCH DAMAGES. THIS LIMITATION SHALL APPLY NOTWITHSTANDING ANY FAILURE OF ESSENTIAL PURPOSE OF ANY LIMITED REMEDY PROVIDED HEREIN.

8. Limitations

8. 1. ***BOOKS ONLY:***Where **'reuse in a dissertation/thesis'** has been selected the following terms apply: Print rights of the final author's accepted manuscript (for clarity,

NOT the published version) for up to 100 copies, electronic rights for use only on a personal website or institutional repository as defined by the Sherpa guideline (www.sherpa.ac.uk/romeo/).

8. 2. For content reuse requests that qualify for permission under the STM Permissions Guidelines, which may be updated from time to time, the STM Permissions Guidelines supersede the terms and conditions contained in this licence.

9. Termination and Cancellation

9. 1. Licences will expire after the period shown in Clause 3 (above).

9. 2. Licensee reserves the right to terminate the Licence in the event that payment is not received in full or if there has been a breach of this agreement by you.

Appendix 1 — Acknowledgements:

For Journal Content:
Reprinted by permission from [**the Licensor**]: [**Journal Publisher** (e.g. Nature/Springer/Palgrave)] [**JOURNAL NAME**] [**REFERENCE CITATION** (Article name, Author(s) Name), [**COPYRIGHT**] (year of publication)

For **Advance Online Publication papers:**
Reprinted by permission from [**the Licensor**]: [**Journal Publisher** (e.g. Nature/Springer/Palgrave)] [**JOURNAL NAME**] [**REFERENCE CITATION** (Article name, Author(s) Name), [**COPYRIGHT**] (year of publication), advance online publication, day month year (doi: 10.1038/sj.[JOURNAL ACRONYM].)

For Adaptations/Translations:
Adapted/Translated by permission from [**the Licensor**]: [**Journal Publisher** (e.g. Nature/Springer/Palgrave)] [**JOURNAL NAME**] [**REFERENCE CITATION** (Article name, Author(s) Name), [**COPYRIGHT**] (year of publication)

Note: For any republication from the British Journal of Cancer, the following credit line style applies:

Reprinted/adapted/translated by permission from [**the Licensor**]: on behalf of Cancer Research UK: : [**Journal Publisher** (e.g. Nature/Springer/Palgrave)] [**JOURNAL NAME**] [**REFERENCE CITATION** (Article name, Author(s) Name), [**COPYRIGHT]** (year of publication)

For **Advance Online Publication** papers:
Reprinted by permission from The [**the Licensor**]: on behalf of Cancer Research UK: [**Journal Publisher** (e.g. Nature/Springer/Palgrave)] [**JOURNAL NAME**] [**REFERENCE CITATION** (Article name, Author(s) Name), [**COPYRIGHT**] (year of publication), advance online publication, day month year (doi: 10.1038/sj.[JOURNAL ACRONYM])

For Book content:
Reprinted/adapted by permission from [**the Licensor**]: [**Book Publisher** (e.g.

Palgrave Macmillan, Springer etc) [**Book Title**] by [**Book author**(s)]
[**COPYRIGHT**] (year of publication)

Other Conditions:

Version 1.3

Questions? customercare@copyright.com or +1-855-239-3415 (toll free in the US) or +1-978-646-2777.

American Physical Society
Reuse and Permissions License

24-May-2022

This license agreement between the American Physical Society ("APS") and Gustavo Chavez Ponce de Leon ("You") consists of your license details and the terms and conditions provided by the American Physical Society and SciPris.

Licensed Content Information

License Number:	**RNP/22/MAY/053998**
License date:	24-May-2022
DOI:	10.1103/PhysRevB.103.L100410
Title:	All-electrical detection of skyrmion lattice state and chiral surface twists
Author:	A. Aqeel et al.
Publication:	Physical Review B
Publisher:	American Physical Society
Cost:	USD $ 0.00

Request Details

Does your reuse require significant modifications: No

Specify intended distribution locations:	Worldwide
Reuse Category:	Reuse in a thesis/dissertation
Requestor Type:	Student
Items for Reuse:	Figures/Tables
Number of Figure/Tables:	2
Figure/Tables Details:	The contour plot
Format for Reuse:	Electronic

Information about New Publication:

University/Publisher:	RUG
Title of dissertation/thesis:	Spin Hall magnetoresistence for electronic determination of magnetic ordering
Author(s):	Gustavo Chavez Ponce de Leon
Expected completion date:	Jun. 2022

License Requestor Information

Name:	Gustavo Chavez Ponce de Leon
Affiliation:	Individual
Email Id:	g.chavez.ponce.de.leon@student.rug.nl
Country:	Netherlands

American Physical Society
Reuse and Permissions License

TERMS AND CONDITIONS

The American Physical Society (APS) is pleased to grant the Requestor of this license a non-exclusive, non-transferable permission, limited to Electronic format, provided all criteria outlined below are followed.

1. You must also obtain permission from at least one of the lead authors for each separate work, if you haven't done so already. The author's name and affiliation can be found on the first page of the published Article.

2. For electronic format permissions, Requestor agrees to provide a hyperlink from the reprinted APS material using the source material's DOI on the web page where the work appears. The hyperlink should use the standard DOI resolution URL, http://dx.doi.org/{DOI}. The hyperlink may be embedded in the copyright credit line.

3. For print format permissions, Requestor agrees to print the required copyright credit line on the first page where the material appears: "Reprinted (abstract/excerpt/figure) with permission from [(FULL REFERENCE CITATION) as follows: Author's Names, APS Journal Title, Volume Number, Page Number and Year of Publication.] Copyright (YEAR) by the American Physical Society."

4. Permission granted in this license is for a one-time use and does not include permission for any future editions, updates, databases, formats or other matters. Permission must be sought for any additional use.

5. Use of the material does not and must not imply any endorsement by APS.

6. APS does not imply, purport or intend to grant permission to reuse materials to which it does not hold copyright. It is the requestor's sole responsibility to ensure the licensed material is original to APS and does not contain the copyright of another entity, and that the copyright notice of the figure, photograph, cover or table does not indicate it was reprinted by APS with permission from another source.

7. The permission granted herein is personal to the Requestor for the use specified and is not transferable or assignable without express written permission of APS. This license may not be amended except in writing by APS.

8. You may not alter, edit or modify the material in any manner.

9. You may translate the materials only when translation rights have been granted.

10. APS is not responsible for any errors or omissions due to translation.

11. You may not use the material for promotional, sales, advertising or marketing purposes.

12. The foregoing license shall not take effect unless and until APS or its agent, Aptara, receives payment in full in accordance with Aptara Billing and Payment Terms and Conditions, which are incorporated herein by reference.

13. Should the terms of this license be violated at any time, APS or Aptara may revoke the license with no refund to you and seek relief to the fullest extent of the laws of the USA. Official written notice will be made using the contact information provided with the permission request. Failure to receive such notice will not nullify revocation of the permission.

14. APS reserves all rights not specifically granted herein.

15. This document, including the Aptara Billing and Payment Terms and Conditions, shall be the entire agreement between the parties relating to the subject matter hereof.

SPRINGER NATURE LICENSE
TERMS AND CONDITIONS

May 24, 2022

This Agreement between RUG -- Gustavo Chavez Ponce de Leon ("You") and Springer Nature ("Springer Nature") consists of your license details and the terms and conditions provided by Springer Nature and Copyright Clearance Center.

License Number	5315370515596
License date	May 24, 2022
Licensed Content Publisher	Springer Nature
Licensed Content Publication	Nature
Licensed Content Title	Real-space observation of a two-dimensional skyrmion crystal
Licensed Content Author	X. Z. Yu et al
Licensed Content Date	Jun 17, 2010
Type of Use	Thesis/Dissertation
Requestor type	academic/university or research institute
Format	electronic
Portion	figures/tables/illustrations
Number of figures/tables/illustrations	1

High-res required	no
Will you be translating?	no
Circulation/distribution	1 - 29
Author of this Springer Nature content	no
Title	Student
Institution name	RUG
Expected presentation date	Jun 2022
Order reference number	001
Portions	Figure 1
Requestor Location	RUG Turfsingel 25A Groningen, 9712KH Netherlands Attn: RUG
Total	0.00 EUR

Terms and Conditions

Springer Nature Customer Service Centre GmbH
Terms and Conditions

This agreement sets out the terms and conditions of the licence (the **Licence**) between you and **Springer Nature Customer Service Centre GmbH** (the **Licensor**). By clicking 'accept' and completing the transaction for the material (**Licensed Material**), you also confirm your acceptance of these terms and conditions.

1. Grant of License

1. 1. The Licensor grants you a personal, non-exclusive, non-transferable, world-wide licence to reproduce the Licensed Material for the purpose specified in your order only. Licences are granted for the specific use requested in the order and for no other use, subject to the conditions below.

1. 2. The Licensor warrants that it has, to the best of its knowledge, the rights to license reuse of the Licensed Material. However, you should ensure that the material you are requesting is original to the Licensor and does not carry the copyright of another entity (as credited in the published version).

1. 3. If the credit line on any part of the material you have requested indicates that it was reprinted or adapted with permission from another source, then you should also seek permission from that source to reuse the material.

2. Scope of Licence

2. 1. You may only use the Licensed Content in the manner and to the extent permitted by these Ts&Cs and any applicable laws.

2. 2. A separate licence may be required for any additional use of the Licensed Material, e.g. where a licence has been purchased for print only use, separate permission must be obtained for electronic re-use. Similarly, a licence is only valid in the language selected and does not apply for editions in other languages unless additional translation rights have been granted separately in the licence. Any content owned by third parties are expressly excluded from the licence.

2. 3. Similarly, rights for additional components such as custom editions and derivatives require additional permission and may be subject to an additional fee. Please apply to Journalpermissions@springernature.com/bookpermissions@springernature.com for these rights.

2. 4. Where permission has been granted **free of charge** for material in print, permission may also be granted for any electronic version of that work, provided that the material is incidental to your work as a whole and that the electronic version is essentially equivalent to, or substitutes for, the print version.

2. 5. An alternative scope of licence may apply to signatories of the STM Permissions Guidelines, as amended from time to time.

3. Duration of Licence

3. 1. A licence for is valid from the date of purchase ('Licence Date') at the end of the relevant period in the below table:

Scope of Licence	Duration of Licence
Post on a website	12 months
Presentations	12 months
Books and journals	Lifetime of the edition in the language purchased

4. Acknowledgement

4. 1. The Licensor's permission must be acknowledged next to the Licenced Material in print. In electronic form, this acknowledgement must be visible at the same time as the figures/tables/illustrations or abstract, and must be hyperlinked to the journal/book's homepage. Our required acknowledgement format is in the Appendix below.

5. Restrictions on use

5. 1. Use of the Licensed Material may be permitted for incidental promotional use and minor editing privileges e.g. minor adaptations of single figures, changes of format, colour and/or style where the adaptation is credited as set out in Appendix 1 below. Any other changes including but not limited to, cropping, adapting, omitting material that affect the meaning, intention or moral rights of the author are strictly prohibited.

5. 2. You must not use any Licensed Material as part of any design or trademark.

5. 3. Licensed Material may be used in Open Access Publications (OAP) before publication by Springer Nature, but any Licensed Material must be removed from OAP sites prior to final publication.

6. Ownership of Rights

6. 1. Licensed Material remains the property of either Licensor or the relevant third party and any rights not explicitly granted herein are expressly reserved.

7. Warranty

IN NO EVENT SHALL LICENSOR BE LIABLE TO YOU OR ANY OTHER PARTY OR ANY OTHER PERSON OR FOR ANY SPECIAL, CONSEQUENTIAL, INCIDENTAL OR INDIRECT DAMAGES, HOWEVER CAUSED, ARISING OUT OF OR IN CONNECTION WITH THE DOWNLOADING, VIEWING OR USE OF THE MATERIALS REGARDLESS OF THE FORM OF ACTION, WHETHER FOR BREACH OF CONTRACT, BREACH OF WARRANTY, TORT, NEGLIGENCE, INFRINGEMENT OR OTHERWISE (INCLUDING, WITHOUT LIMITATION, DAMAGES BASED ON LOSS OF PROFITS, DATA, FILES, USE, BUSINESS OPPORTUNITY OR CLAIMS OF THIRD PARTIES), AND
WHETHER OR NOT THE PARTY HAS BEEN ADVISED OF THE POSSIBILITY OF SUCH DAMAGES. THIS LIMITATION SHALL APPLY NOTWITHSTANDING ANY FAILURE OF ESSENTIAL PURPOSE OF ANY LIMITED REMEDY PROVIDED HEREIN.

8. Limitations

8. 1. ***BOOKS ONLY:***Where **'reuse in a dissertation/thesis'** has been selected the following terms apply: Print rights of the final author's accepted manuscript (for clarity,

NOT the published version) for up to 100 copies, electronic rights for use only on a personal website or institutional repository as defined by the Sherpa guideline (www.sherpa.ac.uk/romeo/).

8. 2. For content reuse requests that qualify for permission under the STM Permissions Guidelines, which may be updated from time to time, the STM Permissions Guidelines supersede the terms and conditions contained in this licence.

9. Termination and Cancellation

9. 1. Licences will expire after the period shown in Clause 3 (above).

9. 2. Licensee reserves the right to terminate the Licence in the event that payment is not received in full or if there has been a breach of this agreement by you.

Appendix 1 — Acknowledgements:

For Journal Content:
Reprinted by permission from [**the Licensor**]: [**Journal Publisher** (e.g. Nature/Springer/Palgrave)] [**JOURNAL NAME**] [**REFERENCE CITATION** (Article name, Author(s) Name), [**COPYRIGHT**] (year of publication)

For **Advance Online Publication papers:**
Reprinted by permission from [**the Licensor**]: [**Journal Publisher** (e.g. Nature/Springer/Palgrave)] [**JOURNAL NAME**] [**REFERENCE CITATION** (Article name, Author(s) Name), [**COPYRIGHT**] (year of publication), advance online publication, day month year (doi: 10.1038/sj.[JOURNAL ACRONYM].)

For Adaptations/Translations:
Adapted/Translated by permission from [**the Licensor**]: [**Journal Publisher** (e.g. Nature/Springer/Palgrave)] [**JOURNAL NAME**] [**REFERENCE CITATION** (Article name, Author(s) Name), [**COPYRIGHT**] (year of publication)

Note: For any republication from the British Journal of Cancer, the following credit line style applies:

Reprinted/adapted/translated by permission from [**the Licensor**]: on behalf of Cancer Research UK: : [**Journal Publisher** (e.g. Nature/Springer/Palgrave)] [**JOURNAL NAME**] [**REFERENCE CITATION** (Article name, Author(s) Name), [**COPYRIGHT]** (year of publication)

For **Advance Online Publication** papers:
Reprinted by permission from The [**the Licensor**]: on behalf of Cancer Research UK: [**Journal Publisher** (e.g. Nature/Springer/Palgrave)] [**JOURNAL NAME**] [**REFERENCE CITATION** (Article name, Author(s) Name), [**COPYRIGHT**] (year of publication), advance online publication, day month year (doi: 10.1038/sj.[JOURNAL ACRONYM])

For Book content:
Reprinted/adapted by permission from [**the Licensor**]: [**Book Publisher** (e.g.

Palgrave Macmillan, Springer etc) [**Book Title**] by [**Book author**(s)]
[**COPYRIGHT**] (year of publication)

Other Conditions:

Version 1.3

Questions? customercare@copyright.com or +1-855-239-3415 (toll free in the US) or +1-978-646-2777.

THE AMERICAN ASSOCIATION FOR THE ADVANCEMENT OF SCIENCE LICENSE TERMS AND CONDITIONS

May 24, 2022

This Agreement between RUG -- Gustavo Chavez Ponce de Leon ("You") and The American Association for the Advancement of Science ("The American Association for the Advancement of Science") consists of your license details and the terms and conditions provided by The American Association for the Advancement of Science and Copyright Clearance Center.

License Number	5315380488411
License date	May 24, 2022
Licensed Content Publisher	The American Association for the Advancement of Science
Licensed Content Publication	Science
Licensed Content Title	Skyrmion Lattice in a Chiral Magnet
Licensed Content Author	S. Mühlbauer, B. Binz, F. Jonietz, C. Pfleiderer, et al.
Licensed Content Date	Feb 13, 2009
Licensed Content Volume	323
Licensed Content Issue	5916
Volume number	323
Issue number	5916
Type of Use	Thesis / Dissertation

Requestor type	Scientist/individual at a research institution
Format	Electronic
Portion	Text Excerpt
Number of pages requested	4
Title	Student
Institution name	RUG
Expected presentation date	Jun 2022
Order reference number	003
Portions	Only Figures
Requestor Location	RUG Turfsingel 25A Groningen, 9712KH Netherlands Attn: RUG
Total	0.00 USD

Terms and Conditions

American Association for the Advancement of Science TERMS AND CONDITIONS

Regarding your request, we are pleased to grant you non-exclusive, non-transferable permission, to republish the AAAS material identified above in your work identified above, subject to the terms and conditions herein. We must be contacted for permission for any uses other than those specifically identified in your request above.

The following credit line must be printed along with the AAAS material: "From [Full Reference Citation]. Reprinted with permission from AAAS."

All required credit lines and notices must be visible any time a user accesses any part of the AAAS material and must appear on any printed copies and authorized user might make.

This permission does not apply to figures / photos / artwork or any other content or materials included in your work that are credited to non-AAAS sources. If the requested material is sourced to or references non-AAAS sources, you must obtain authorization from that source as well before using that material. You agree to hold harmless and indemnify AAAS against any claims arising from your use of any content in your work that is credited to non-AAAS sources.

If the AAAS material covered by this permission was published in Science during the years 1974 - 1994, you must also obtain permission from the author, who may grant or withhold permission, and who may or may not charge a fee if permission is granted. See original article for author's address. This condition does not apply to news articles.

The AAAS material may not be modified or altered except that figures and tables may be modified with permission from the author. Author permission for any such changes must be secured prior to your use.

Whenever possible, we ask that electronic uses of the AAAS material permitted herein include a hyperlink to the original work on AAAS's website (hyperlink may be embedded in the reference citation).

AAAS material reproduced in your work identified herein must not account for more than 30% of the total contents of that work.

AAAS must publish the full paper prior to use of any text.

AAAS material must not imply any endorsement by the American Association for the Advancement of Science.

This permission is not valid for the use of the AAAS and/or Science logos.

AAAS makes no representations or warranties as to the accuracy of any information contained in the AAAS material covered by this permission, including any warranties of

merchantability or fitness for a particular purpose.

If permission fees for this use are waived, please note that AAAS reserves the right to charge for reproduction of this material in the future.

Permission is not valid unless payment is received within sixty (60) days of the issuance of this permission. If payment is not received within this time period then all rights granted herein shall be revoked and this permission will be considered null and void.

In the event of breach of any of the terms and conditions herein or any of CCC's Billing and Payment terms and conditions, all rights granted herein shall be revoked and this permission will be considered null and void.

AAAS reserves the right to terminate this permission and all rights granted herein at its discretion, for any purpose, at any time. In the event that AAAS elects to terminate this permission, you will have no further right to publish, publicly perform, publicly display, distribute or otherwise use any matter in which the AAAS content had been included, and all fees paid hereunder shall be fully refunded to you. Notification of termination will be sent to the contact information as supplied by you during the request process and termination shall be immediate upon sending the notice. Neither AAAS nor CCC shall be liable for any costs, expenses, or damages you may incur as a result of the termination of this permission, beyond the refund noted above.

This Permission may not be amended except by written document signed by both parties.

The terms above are applicable to all permissions granted for the use of AAAS material. Below you will find additional conditions that apply to your particular type of use.

FOR A THESIS OR DISSERTATION
If you are using figure(s)/table(s), permission is granted for use in print and electronic versions of your dissertation or thesis. A full text article may be used in print versions only of a dissertation or thesis.

Permission covers the distribution of your dissertation or thesis on demand by ProQuest / UMI, provided the AAAS material covered by this permission remains in situ.

If you are an Original Author on the AAAS article being reproduced, please refer to your License to Publish for rules on reproducing your paper in a dissertation or thesis.

FOR JOURNALS:
Permission covers both print and electronic versions of your journal article, however the AAAS material may not be used in any manner other than within the context of your article.

FOR BOOKS/TEXTBOOKS:
If this license is to reuse figures/tables, then permission is granted for non-exclusive world rights in all languages in both print and electronic formats (electronic formats are defined below).

If this license is to reuse a text excerpt or a full text article, then permission is granted for non-exclusive world rights in English only. You have the option of securing either print or electronic rights or both, but electronic rights are not automatically granted and do garner additional fees. Permission for translations of text excerpts or full text articles into other languages must be obtained separately.

Licenses granted for use of AAAS material in electronic format books/textbooks are valid only in cases where the electronic version is equivalent to or substitutes for the print version of the book/textbook. The AAAS material reproduced as permitted herein must remain in situ and must not be exploited separately (for example, if permission covers the use of a full text article, the article may not be offered for access or for purchase as a stand-alone unit), except in the case of permitted textbook companions as noted below.

You must include the following notice in any electronic versions, either adjacent to the reprinted AAAS material or in the terms and conditions for use of your electronic products: "Readers may view, browse, and/or download material for temporary copying purposes only, provided these uses are for noncommercial personal purposes. Except as provided by law, this material may not be further reproduced, distributed, transmitted, modified, adapted, performed, displayed, published, or sold in whole or in part, without prior written permission from the publisher."

If your book is an academic textbook, permission covers the following companions to your textbook, provided such companions are distributed only in conjunction with your textbook at no additional cost to the user:

- Password-protected website
- Instructor's image CD/DVD and/or PowerPoint resource
- Student CD/DVD

All companions must contain instructions to users that the AAAS material may be used for non-commercial, classroom purposes only. Any other uses require the prior written permission from AAAS.

If your license is for the use of AAAS Figures/Tables, then the electronic rights granted herein permit use of the Licensed Material in any Custom Databases that you distribute the electronic versions of your textbook through, so long as the Licensed Material remains within the context of a chapter of the title identified in your request and cannot be downloaded by a user as an independent image file.

Rights also extend to copies/files of your Work (as described above) that you are required to provide for use by the visually and/or print disabled in compliance with state and federal laws.

This permission only covers a single edition of your work as identified in your request.

FOR NEWSLETTERS:
Permission covers print and/or electronic versions, provided the AAAS material reproduced as permitted herein remains in situ and is not exploited separately (for example, if permission covers the use of a full text article, the article may not be offered for access or for purchase as a stand-alone unit)

FOR ANNUAL REPORTS:
Permission covers print and electronic versions provided the AAAS material reproduced as permitted herein remains in situ and is not exploited separately (for example, if permission covers the use of a full text article, the article may not be offered for access or for purchase as a stand-alone unit)

FOR PROMOTIONAL/MARKETING USES:
Permission covers the use of AAAS material in promotional or marketing pieces such as information packets, media kits, product slide kits, brochures, or flyers limited to a single print run. The AAAS Material may not be used in any manner which implies endorsement or promotion by the American Association for the Advancement of Science (AAAS) or Science of any product or service. AAAS does not permit the reproduction of its name, logo or text on promotional literature.

If permission to use a full text article is permitted, The Science article covered by this permission must not be altered in any way. No additional printing may be set onto an article copy other than the copyright credit line required above. Any alterations must be approved in advance and in writing by AAAS. This includes, but is not limited to, the placement of sponsorship identifiers, trademarks, logos, rubber stamping or self-adhesive stickers onto the article copies.

Additionally, article copies must be a freestanding part of any information package (i.e. media kit) into which they are inserted. They may not be physically attached to anything, such as an advertising insert, or have anything attached to them, such as a sample product. Article copies must be easily removable from any kits or informational packages in which they are used. The only exception is that article copies may be inserted into three-ring binders.

FOR CORPORATE INTERNAL USE:
The AAAS material covered by this permission may not be altered in any way. No additional printing may be set onto an article copy other than the required credit line. Any alterations must be approved in advance and in writing by AAAS. This includes, but is not

limited to the placement of sponsorship identifiers, trademarks, logos, rubber stamping or self-adhesive stickers onto article copies.

If you are making article copies, copies are restricted to the number indicated in your request and must be distributed only to internal employees for internal use.

If you are using AAAS Material in Presentation Slides, the required credit line must be visible on the slide where the AAAS material will be reprinted

If you are using AAAS Material on a CD, DVD, Flash Drive, or the World Wide Web, you must include the following notice in any electronic versions, either adjacent to the reprinted AAAS material or in the terms and conditions for use of your electronic products: "Readers may view, browse, and/or download material for temporary copying purposes only, provided these uses are for noncommercial personal purposes. Except as provided by law, this material may not be further reproduced, distributed, transmitted, modified, adapted, performed, displayed, published, or sold in whole or in part, without prior written permission from the publisher." Access to any such CD, DVD, Flash Drive or Web page must be restricted to your organization's employees only.

FOR CME COURSE and SCIENTIFIC SOCIETY MEETINGS:
Permission is restricted to the particular Course, Seminar, Conference, or Meeting indicated in your request. If this license covers a text excerpt or a Full Text Article, access to the reprinted AAAS material must be restricted to attendees of your event only (if you have been granted electronic rights for use of a full text article on your website, your website must be password protected, or access restricted so that only attendees can access the content on your site).

If you are using AAAS Material on a CD, DVD, Flash Drive, or the World Wide Web, you must include the following notice in any electronic versions, either adjacent to the reprinted AAAS material or in the terms and conditions for use of your electronic products: "Readers may view, browse, and/or download material for temporary copying purposes only, provided these uses are for noncommercial personal purposes. Except as provided by law, this material may not be further reproduced, distributed, transmitted, modified, adapted, performed, displayed, published, or sold in whole or in part, without prior written permission from the publisher."

FOR POLICY REPORTS:
These rights are granted only to non-profit organizations and/or government agencies. Permission covers print and electronic versions of a report, provided the required credit line appears in both versions and provided the AAAS material reproduced as permitted herein remains in situ and is not exploited separately.

FOR CLASSROOM PHOTOCOPIES:
Permission covers distribution in print copy format only. Article copies must be freestanding and not part of a course pack. They may not be physically attached to anything or have anything attached to them.

FOR COURSEPACKS OR COURSE WEBSITES:
These rights cover use of the AAAS material in one class at one institution. Permission is valid only for a single semester after which the AAAS material must be removed from the Electronic Course website, unless new permission is obtained for an additional semester. If the material is to be distributed online, access must be restricted to students and instructors enrolled in that particular course by some means of password or access control.

FOR WEBSITES:
You must include the following notice in any electronic versions, either adjacent to the reprinted AAAS material or in the terms and conditions for use of your electronic products: "Readers may view, browse, and/or download material for temporary copying purposes only, provided these uses are for noncommercial personal purposes. Except as provided by law, this material may not be further reproduced, distributed, transmitted, modified, adapted, performed, displayed, published, or sold in whole or in part, without prior written permission from the publisher."

Permissions for the use of Full Text articles on third party websites are granted on a case by case basis and only in cases where access to the AAAS Material is restricted by some means of password or access control. Alternately, an E-Print may be purchased through our reprints department (brocheleau@rockwaterinc.com).

REGARDING FULL TEXT ARTICLE USE ON THE WORLD WIDE WEB IF YOU ARE AN 'ORIGINAL AUTHOR' OF A SCIENCE PAPER

If you chose "Original Author" as the Requestor Type, you are warranting that you are one of authors listed on the License Agreement as a "Licensed content author" or that you are acting on that author's behalf to use the Licensed content in a new work that one of the authors listed on the License Agreement as a "Licensed content author" has written.

Original Authors may post the 'Accepted Version' of their full text article on their personal or on their University website and not on any other website. The 'Accepted Version' is the version of the paper accepted for publication by AAAS including changes resulting from peer review but prior to AAAS's copy editing and production (in other words not the AAAS published version).

FOR MOVIES / FILM / TELEVISION:
Permission is granted to use, record, film, photograph, and/or tape the AAAS material in connection with your program/film and in any medium your program/film may be shown or heard, including but not limited to broadcast and cable television, radio, print, world wide web, and videocassette.

The required credit line should run in the program/film's end credits.

FOR MUSEUM EXHIBITIONS:
Permission is granted to use the AAAS material as part of a single exhibition for the duration of that exhibit. Permission for use of the material in promotional materials for the exhibit must be cleared separately with AAAS (please contact us at permissions@aaas.org).

FOR TRANSLATIONS:
Translation rights apply only to the language identified in your request summary above.

The following disclaimer must appear with your translation, on the first page of the article, after the credit line: "This translation is not an official translation by AAAS staff, nor is it endorsed by AAAS as accurate. In crucial matters, please refer to the official English-language version originally published by AAAS."

FOR USE ON A COVER:
Permission is granted to use the AAAS material on the cover of a journal issue, newsletter issue, book, textbook, or annual report in print and electronic formats provided the AAAS material reproduced as permitted herein remains in situ and is not exploited separately

By using the AAAS Material identified in your request, you agree to abide by all the terms and conditions herein.

Questions about these terms can be directed to the AAAS Permissions department permissions@aaas.org.

Other Terms and Conditions:

v 2

Questions? customercare@copyright.com or +1-855-239-3415 (toll free in the US) or +1-978-646-2777.